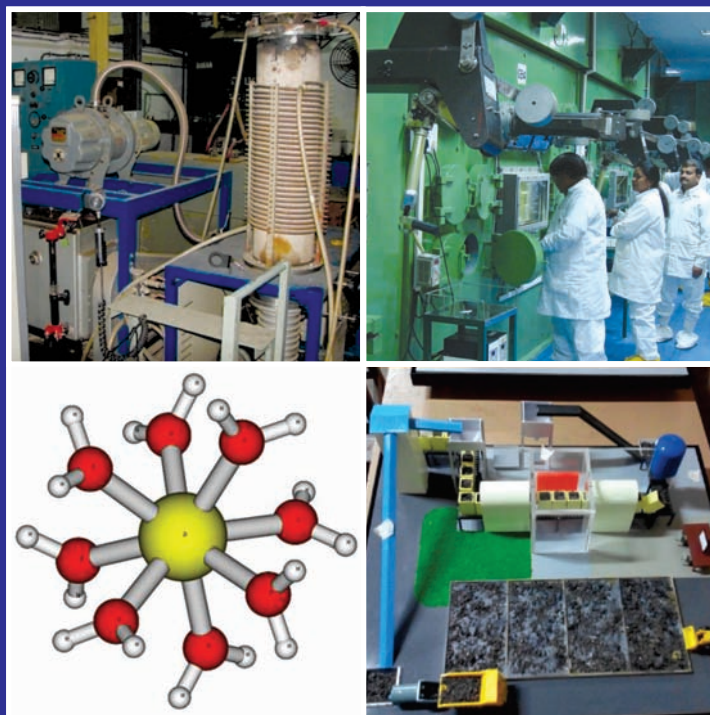


BARC

NEWSLETTER



भाभा परमाणु अनुसंधान केंद्र
BHABHA ATOMIC RESEARCH CENTRE



IN THIS ISSUE

- Development and Characterization of (Ti,Cr)B₂ based Composites
- Design and screening of extractants for Zr⁴⁺-Hf⁴⁺ separation: Synergistic approach using molecular modelling and solvent extraction
- Radiation Technology for Sewage Sludge Hygienisation
- Design of Sealing Arrangements for Development of Leak Tight Articulated Manipulator For Waste Management and Reprocessing Plants
- Optimization of Indigenously Developed Column for the Separation and Analysis of All the Six Hydrogen Isotopic Combinations in Elemental form using Gas Chromatograph

Editorial Committee

Chairman

Dr. S.M. Sharma
Physics Group

Co-Chairman

Dr. G.K. Dey
Materials Group

Editor

Dr. G. Ravi Kumar
SIRD

Associate Editors

Dr. C.P. Kaushik, WMD
Dr. J.B. Singh, MMD

Members

Dr. G. Rami Reddy, RSD
Dr. A.K. Tyagi, Chemistry Divn.
Dr. S.M. Yusuf, SSPD
Dr. S. Kannan, FCD
Dr. C.P. Kaushik, WMD
Dr. S. Mukhopadhyay,
Seismology Divn.
Dr. A.K. Bhattacharjee, RCnD
Dr. B.K. Sapra, RP&AD
Dr. J.B. Singh, MMD
Dr. K.G. Bhushan, TPD
Dr. S. Mukhopadhyay, ChED
Dr. S.K. Sandur, RB&HSD
Dr. Smt. S.C. Deokathey, SIRD

CONTENTS

Research Articles

- Development and Characterization of (Ti,Cr)B₂ based Composites 1
T.S.R.Ch. Murthy, J.K. Sonber, K.Sairam, R.D. Bedse and J.K. Chakravartty

Technology Development Articles

- Design of Sealing Arrangements for Development of Leak Tight Articulated Manipulator For Waste Management and Reprocessing Plants 11
Satish B. Patil and Avinash K. Mudaiya
- Design and screening of extractants for Zr⁴⁺-Hf⁴⁺ separation: Synergistic approach using molecular modelling and solvent extraction 17
Sk. Musharaf Ali, A. Boda, G. Pandey, R. Singh, M. Paramanik, S.K.Ghosh, S. Mukhopadhyay and K.T. Shenoy
- Optimization of Indigenously Developed Column for the Separation and Analysis of All the Six Hydrogen Isotopic Combinations in Elemental form using Gas Chromatograph 23
M. Ravichandran, P.R. Ramya, S. Sankar Ganesh, K. Ramesh Naidu and M.M. Rajput
- Radiation Technology for Sewage Sludge Hygienisation 27
Lalit Varshney

News & Events

- Technology Transfer 32
- 20th National Seminar On Crystal Growth & Applications 2016 (NSCGA-2016): A Report 37

Development and Characterization of (Ti,Cr)B₂ based Composites

T.S.R.Ch. Murthy, J.K. Sonber, K.Sairam and R.D. Bedse

Materials Processing Division

and

J.K. Chakravartty

Materials Group

Abstract

Process flow sheet for the development of (Ti,Cr)B₂ + MoSi₂ composites by hot pressing have been established. The hot pressing operations have been optimized to obtain near theoretical dense (~99%) pellets. Detailed evaluation of mechanical, physical and oxidation behavior of composites with varying CrB₂ content was carried out. (Ti,Cr)B₂ + MoSi₂ composites has been found to have a higher hardness, better fracture toughness and oxidation resistance compared to monolithic TiB₂. These pellets prepared meet all the specifications for use as control rod material of a high temperature/compact nuclear reactor.

Introduction

Boron and its compounds are extensively used in nuclear industry for application as control rod, human shielding against neutrons and as sensor elements [1,2]. Neutron absorption of boron is sufficiently high in the thermal neutron energy range (~3800 barns for ¹⁰B isotope) to make it a candidate for use in advanced/compact/high temperature nuclear reactors as neutron shielding and control/shutoff rods. At higher energies, the cross section of most other neutron absorber elements becomes very small, often abruptly as in the case of cadmium, whereas the cross-section of ¹⁰B decreases monotonically with respect to increase in neutron energy. Absolute values along the entire energy spectrum are of sufficient magnitude to make it very effective in the intermediate and fast energy range of neutrons. Boron has another advantage over other potential neutron absorber materials as the reaction products namely helium (α) and lithium are formed as stable, non-radioactive isotopes. As they do not emit nuclear radiation, decay-heating problems are minimal during reactor shutdowns and transfer of depleted control rods. Elemental boron and boron based compounds boric acid, boron carbide and titanium diboride are the most important substances widely used in nuclear industry [1,2].

Titanium diboride (TiB₂) based composites are chosen as the candidate material for neutron absorption in high temperature/compact reactors due to its high temperature properties. TiB₂ has high melting point (3200°C), low

density (4.52 gm/cm³), good thermal conductivity (65 W/m/K), chemical inertness and moderate oxidation resistance. Covalent nature of the TiB₂ compound coupled with low diffusion coefficient makes it extremely difficult to obtain dense bodies by sintering. In real high temperature applications monolithic TiB₂ directly cannot be used, due to its poor sinterability, oxidation and thermal shock resistance. However, these difficulties can be overcome by adding suitable sinter additives. In the present study focuses on the development of TiB₂ based composite of "(Ti,Cr)B₂+20% MoSi₂" and evaluation of thermo physical (CTE, electrical resistivity), mechanical (hardness, fracture toughness, flexural strength, hot hardness) and high temperature oxidation (isothermal and continuous) properties.

In addition to the above said composite, authors have also successfully developed and characterized the various refractory and rare earth metal borides (TiB₂, CrB₂, ZrB₂, HfB₂, EuB₆, LaB₆, CeB₆, YB₄, NbB₂) and its composites. More details on synthesis, densification and properties of these borides are found elsewhere [3-15]. Literature reported properties of B₄C, TiB₂, CrB₂ and MoSi₂ are summarized in Table 1[1,2,5,6,7].

Development of (Ti,Cr)B₂ and MoSi₂ composites

(Ti,Cr)B₂ and MoSi₂ are synthesized independently and a mixture of these powders in the required proportion is hot pressed to obtain the dense pellets. However, during the developmental process, synthesis of TiB₂ and CrB₂ were

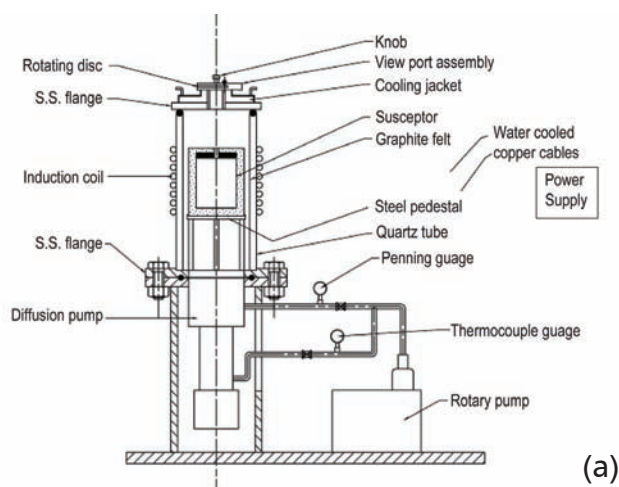
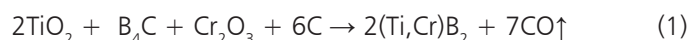
Table.1 Comparison of properties of selected materials (B_4C , TiB_2 , CrB_2 , $MoSi_2$) [1,2,5,6,7]

Property	B_4C	TiB_2	CrB_2	$MoSi_2$
Melting point ($^{\circ}C$)	2450	3200	2200	2030
Thermal conductivity (W/m/K)	30 - 42	60 - 120	30-35	53.92
Density (g/cc)	2.51	4.52	5.2	6.24
Hardness (GPa)	28	32	11–20	12
Coefficient of Thermal Expansion ($^{\circ}C^{-1}$)	5×10^{-6}	8.1×10^{-6}	10.5×10^{-6}	8.5×10^{-6}
Oxidation resistance upto	$\leq 800^{\circ}C$	$\leq 1000^{\circ}C$	-	$\leq 1400^{\circ}C$
Strength (MPa)	155	240	207-600	-
Fracture toughness (K_{IC}) MPa.m $^{1/2}$	2-3	5-7	3-4	3-4
Electrical resistivity ($\mu\Omega - cm$)	$0.1-10 \times 10^6$	10 – 30	-	21.6

studied separately to evolve the production process for composite borides. Optimization of process parameters for the production of $(Ti,Cr)B_2$ & $MoSi_2$ and hot pressing of the mixture of these powders to obtain dense pellet were also established. Important process steps are explained below:

Synthesis of pre-alloyed titanium, chromium di-boride [$(Ti_{0.85}Cr_{0.15})B_2$]

Our previous studies indicated that synthesis of TiB_2 and CrB_2 require temperatures above $1700^{\circ}C$ for obtaining single phase compound [14,15] with minimum impurities of $< 1\%$. Synthesis of the pre-alloyed composite boride [$(Ti,Cr)B_2$] by co-reduction technique in a single step is considered to be advantageous and economical in obtaining a homogenous product with improved properties compared to ex-situ processing route. Hence, synthesis of $(Ti,Cr)B_2$ was carried out by the following carbothermic reduction in the presence of boron carbide:



This carbide-oxide reaction is the simplest method of preparing compounds, when the reactants are available in pure and finely divided form. As the reactants consist of four solid substances, homogenization of the charge mixture is essential for completion of the reaction. Fine powders of reactants are accurately weighed and mixed thoroughly by planetary mill. Mixed charge is loaded into a graphite crucible and heated in a vacuum induction furnace. Fig.1 shows the schematic and actual photograph of vacuum induction furnace assembly used in the present study. Temperature of the furnace was measured by two color pyrometer. After completion of holding time, the furnace was allowed to cool down to room temperature in vacuum. Synthesized compacts were taken out, crushed and ground to fine particles using WC lined high energy cup grinding mill. XRD of the powders were taken for phase identification and chemical analysis for the major constituents and impurities. Particle size analysis was carried out by laser scattering method. SEM of the powders was carried out to cross check the particle size and morphology.



Fig.1: a) Schematic and b) actual photograph of a vacuum induction furnace used for synthesis of $(Ti,Cr)B_2$ and $MoSi_2$

Synthesis of molybdenum di-silicide (MoSi₂)

MoSi₂ used in the present study was synthesized from its elements. Stoichiometric amounts of molybdenum (Mo, Purity: 99.7%) and silicon (Si, Purity: 99%) powders were weighed and thoroughly mixed in a planetary ball mill. The charge was heated in vacuum up to a temperature of 1300°C. Since the formation of MoSi₂ ($\Delta H_{30^\circ C}^\circ = -131$ kJ/mol) is highly exothermic, abrupt increase in the charge temperature was observed, which indicates the vigorous reaction in the charge.

Consolidation of pellets

Fine powders of (Ti,Cr)B₂ and MoSi₂ are weighed in the specified proportion and mixed thoroughly in a gyratory mixer. All these operations are carried out using tungsten

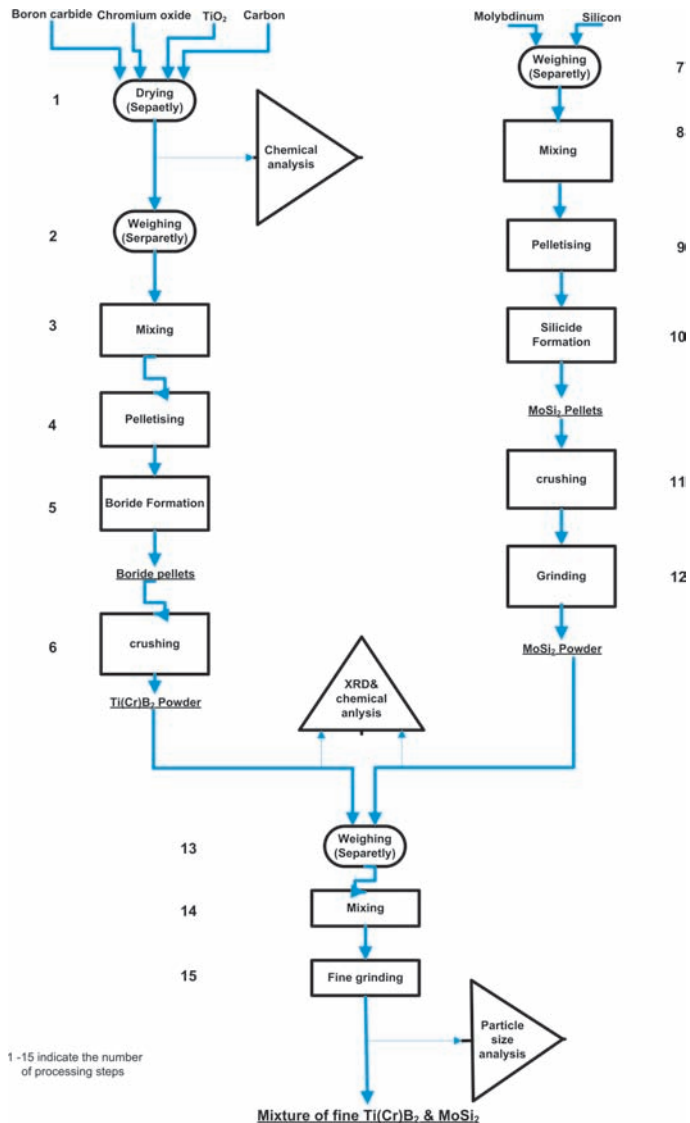


Fig. 2: Flow sheet for the preparation of (Ti,Cr)B₂ and MoSi₂ powder mixture



Fig. 3: Planetary ball mill used for mixing of starting powders

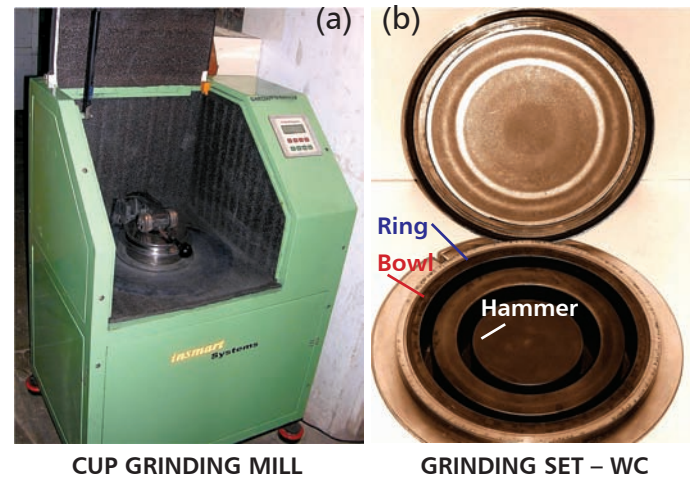


Fig. 4: a) Photograph of a vibratory cup grinding mill and b) WC lined bowl set

carbide lined mills to avoid contamination from milling medium during powder processing. Flow sheet for the preparation of composite powders of fine (Ti,Cr)B₂ and MoSi₂ for boron alloy preparation are presented in Fig.2. Fig.3 and Fig.4 are showing the photographs of planetary and high energy cup grinding mill used for mixing and fine grinding. Particle size distribution and XRD patterns of starting (Ti,Cr)B₂, MoSi₂ and mixed powder are presented in Fig.5 and Fig 6 (a&b) respectively.

Densification of (Ti,Cr)B₂+MoSi₂ composites were carried out by hot pressing. For hot pressing experiments, weighed

quantities of $(Ti,Cr)B_2$ (5,10 and 15wt.% CrB_2 equivalent powders) and 20 wt.% $MoSi_2$ powders were mixed thoroughly using a motorized pestle and mortar in dry condition for 1 h. The powders were then uniaxially pressed using a graphite die of 12 mm diameter at $1800^\circ C$ under pressure (35 MPa) for 1 hour in a vacuum of 0.01 pascal. The densified pellets were ejected from the die and the density measured by Archimedes' principle. Schematic and actual photograph of hot press used for present study is presented in Fig.7.

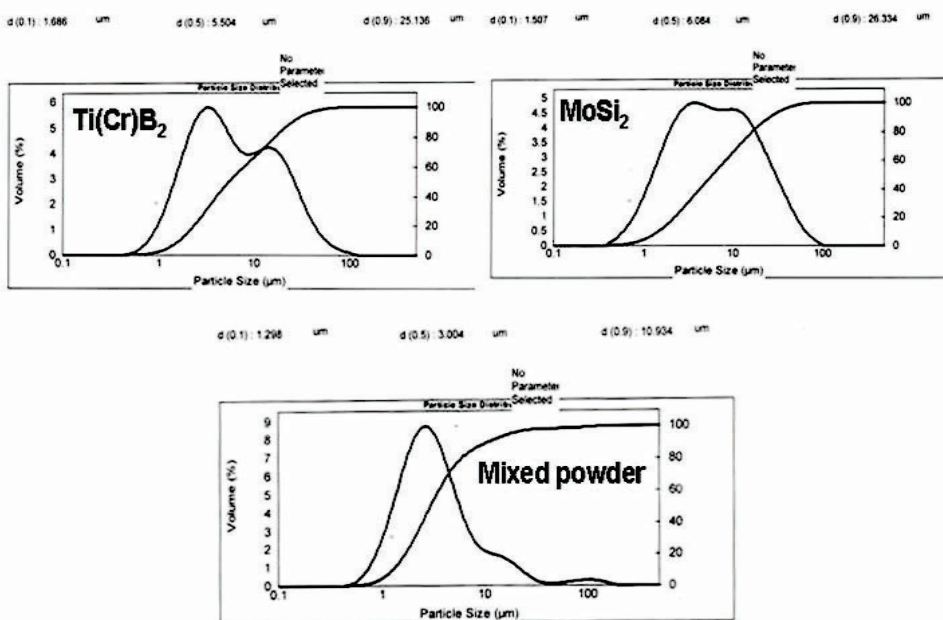


Fig. 5: Particle size distribution of $(Ti_{0.85}Cr_{0.15})B_2$, $MoSi_2$ and mixed powder [Reprinted from [6] with permission from Elsevier]

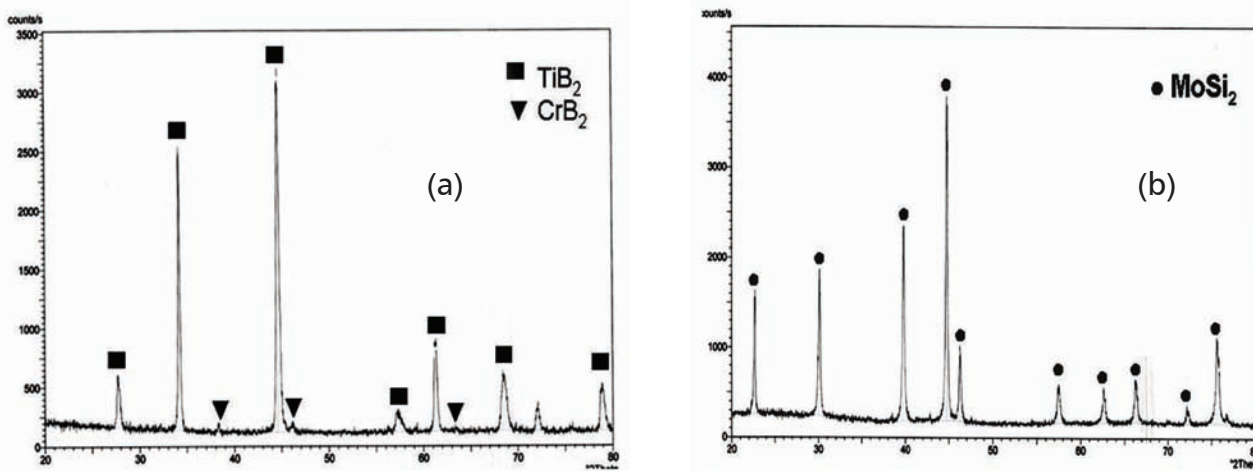


Fig. 6: XRD of a) $(Ti_{0.85}Cr_{0.15})B_2$ and b) $MoSi_2$ powder [Reprinted from [6] with permission from Elsevier]

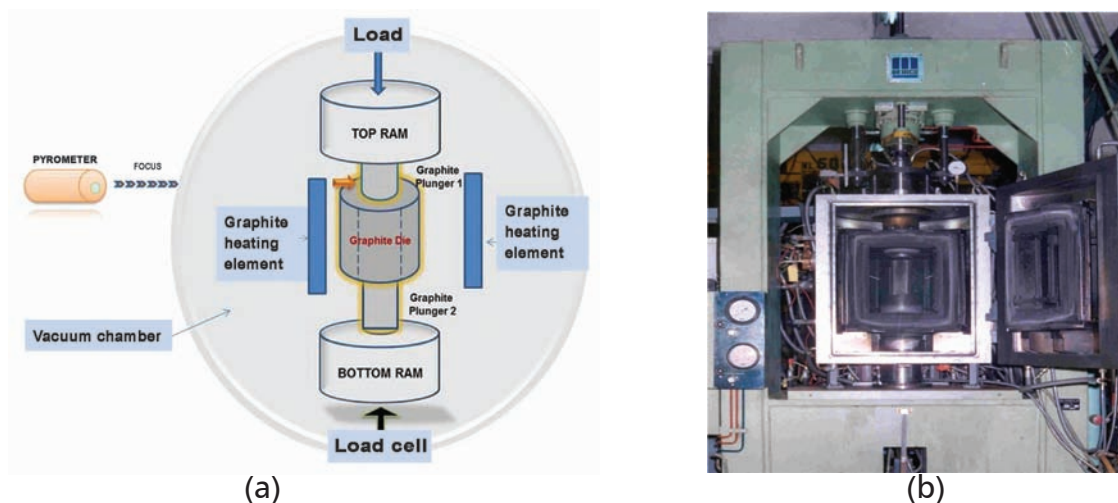


Fig. 7: a) Schematic and b) actual photograph of High Temperature and High Vacuum Hot Press used for consolidation of $(Ti,Cr)B_2 + MoSi_2$ composite dense pellets

Characterization of pellets

Densified pellets were cut by using electro discharge machine (EDM) and polished to 0.10 μm finish. X-ray Diffraction (XRD) and Electron Probe Micro Analyser (EPMA) were carried out on the polished surface. Hardness at various temperatures and fracture toughness at room temperature were measured. Thermal conductivity, coefficient of thermal expansion (CTE) and flexural strength were measured using 5mm × 5mm × 45 mm sized bar samples. Fractured surface was examined in a SEM. Isothermal and continuous oxidation studies were also carried out. Detailed results are given below:

Densification

The density of composites obtained with 5, 10 and 15% CrB₂ contained (Ti,Cr)B₂ + 20% MoSi₂ composites were 4.43, 4.67 and 4.81 g/cc respectively. Fig. 8a presents the variation of relative density of pellets with respect to CrB₂ content.

Phase identification

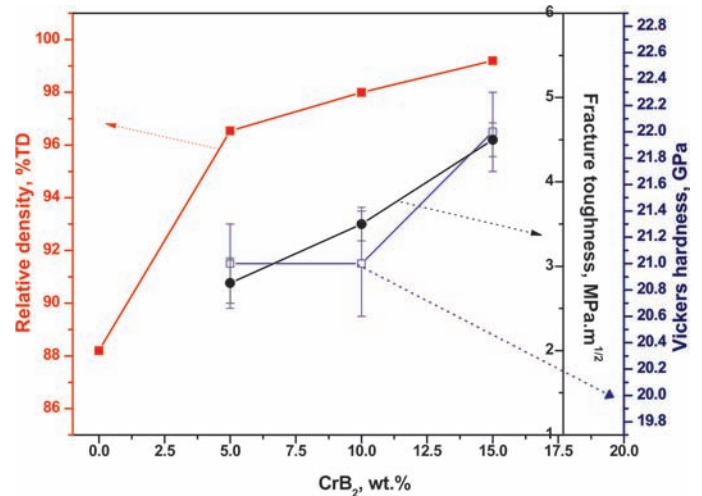
TiB₂ and MoSi₂ peaks are mainly identified and CrB₂ peaks are not seen in the XRD pattern (Fig. 8b). (Ti_{0.85}Cr_{0.15})B₂ + 20% MoSi₂ composite was analyzed by SEM-EDS and EPMA. In this sample, three regions of interest were identified. These are the light grey matrix of (Ti_{0.85}Cr_{0.15})B₂, white phase (MoSi₂) and tiny black phase mainly contains Cr, Ti, Mo and B (Fig 9a). Both intergranular and transgranular modes of fractures contribute equally to the failure of the (Ti_{0.85}Cr_{0.15})B₂ + 20% MoSi₂ composites (SEM images not shown). No grain growth and porosity is observed, indicates the full densification of the composites without grain coarsening.

Mechanical Properties

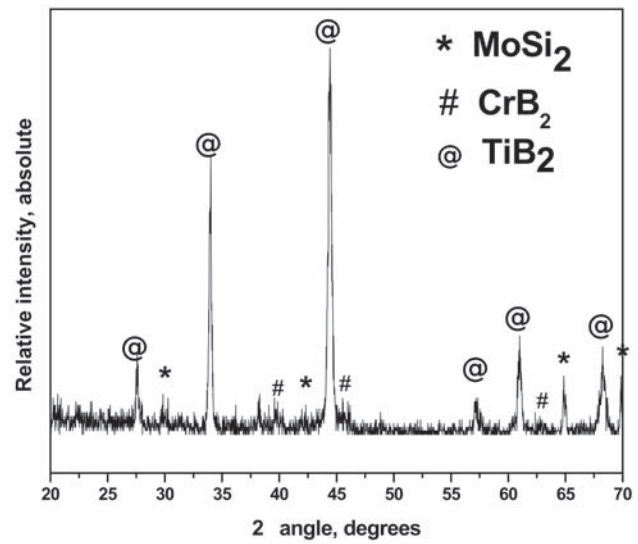
Fig.8a presents the micro hardness and indentation fracture toughness values of the composites with varying the CrB₂ content. Hardness values of all composites are in the range of 24 to 27 GPa. Fracture toughness values were calculated by using the Anstis empirical relation as follows [16]:

$$K_{Ic} = 0.016 (E/H)^{1/2} \times (P/C^{3/2}) \quad (2)$$

Where K_{Ic} is the fracture toughness (MPa.m^{1/2}), E – Elastic modulus (GPa), H – hardness (GPa), P – load (N), 2C – full crack length (m). Elastic modulus of (Ti_{0.85}Cr_{0.15})B₂ + 20% MoSi₂ composite was measured as 522 ± 8 GPa at room temperature by ultrasonic method as per the



(a)



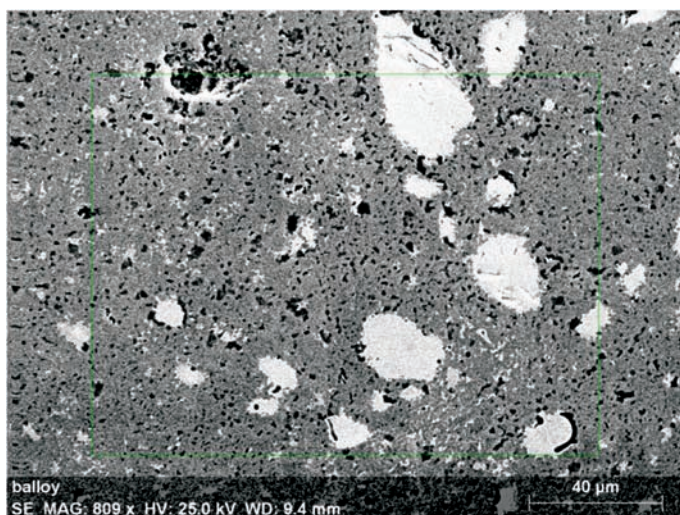
(b)

Fig. 8: a) Relative density, hardness and fracture toughness of boron alloy with varying the CrB₂. b) Phase identification of hot pressed pellet of (Ti_{0.85}Cr_{0.15})B₂ + 20%MoSi₂

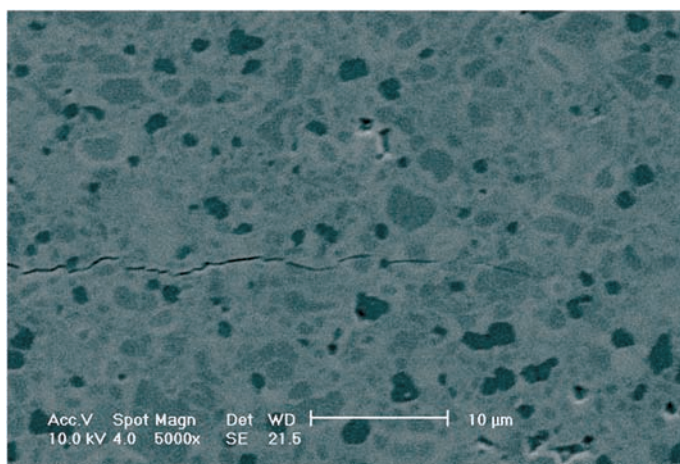
ASTM C1419-99a test procedure. Average indentation fracture toughness of 5, 10 and 15% CrB₂ contained (Ti,Cr)B₂ + 20% MoSi₂ composites were measured as 2.8 ± 0.2, 3.5 ± 0.6 and 4.5 ± 0.5 MPa.m^{1/2} respectively. Hardness of (Ti_{0.85}Cr_{0.15})B₂ + 20% MoSi₂ sample from 25°C to 1000°C is also measured. As expected, with increase in temperature, decrease in hardness values were noted. Drastic decrease in the hardness value from 30GPa to 16GPa was observed from 25°C to 300°C[6]. Flexural strength was measured at RT, 500 and 900°C for (Ti_{0.85}Cr_{0.15})B₂ + 20% MoSi₂ sample. Three samples were tested at each temperature and the average values were 320, 295 and 285 MPa respectively. Similar to hot hardness, decrease in flexural strength values with increase in temperature was noticed. However, decrease

in strength is not significant, indicating the retention of strength at elevated temperature of 900 °C.

Microstructures of $(Ti,Cr)B_2+20\%MoSi_2$ composites with indentation edge cracks are shown in Fig.9b. Both crack deflections and bridging mechanisms were mainly observed in this composite. These mechanisms are responsible for improvement of the fracture toughness [6].



(a)



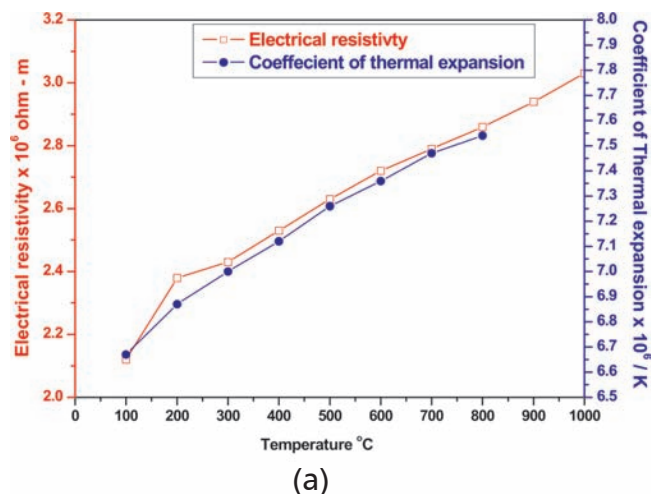
(b)

Fig. 9a) SEM image of polished $(Ti_{0.85}Cr_{0.15})B_2 + 20\%MoSi_2$ composite; b) crack propagation pattern indicates the deflections and bridging mechanisms

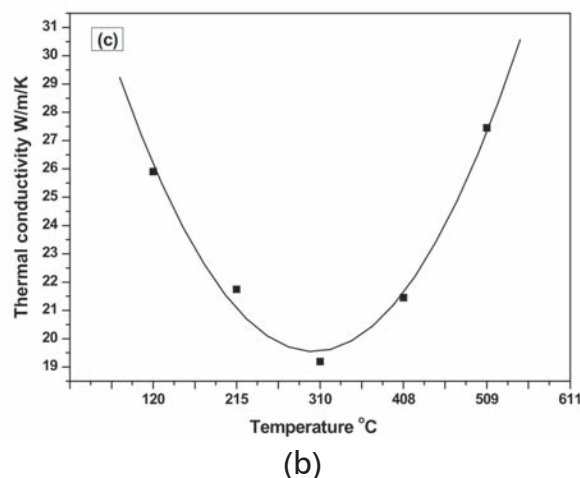
Physical Properties

Coefficient of thermal expansion (CTE) and electrical resistivity of $(Ti_{0.85}Cr_{0.15})B_2 + 20\% MoSi_2$ composite is presented in Fig.10a. CTE values are found to increase with temperature from 6.67×10^{-6} at 100°C to $7.54 \times 10^{-6} K^{-1}$ at 800°C. These values are marginally lower than that of monolithic TiB_2 which is $8.1 \times 10^{-6} K^{-1}$. Electrical resistivity of the composite

was measured as 2.12, 2.63 and $3.03 \mu\Omega -cm$ at 100°C, 500°C and 1000°C respectively. Thermal conductivity of $(Ti_{0.85}Cr_{0.15})B_2 + 20\% MoSi_2$ composite measured up to 600°C and is shown in Fig.10b. Thermal conductivity of sample was observed to decrease from room temperature to 300°C and then increase with temperature. This could be the change in the mechanism of thermal conductivity.



(a)



(b)

Fig. 10: a) Coefficient of thermal expansion and electrical resistivity data of $(Ti_{0.85}Cr_{0.15})B_2 + 20\% MoSi_2$ composite evaluated in inert atmosphere b) Thermal conductivity data of $(Ti_{0.85}Cr_{0.15})B_2 + 20\% MoSi_2$ composite evaluated in inert atmosphere [Reprinted from [6] with permission from Elsevier]

Oxidation Studies

Continuous Oxidation (Non-Isothermal)

TGA plot on continuous oxidation of all $(Ti,Cr)B_2 + 20\%MoSi_2$ composites in O_2 is given in Fig.11a. In the plot, three different stages of weight gain are observed for all the composites, a) no change in sample weight up to 300°C, b)

a gradual weight gain between 300 to 700°C and c) a steep weight gain above 700°C. Total specific weight gain is less than 25×10^{-3} kg/m² and the rate of weight gain is similar for all the composites. It is seen that $(\text{Ti}_{0.85}\text{Cr}_{0.15})\text{B}_2 + 20\% \text{MoSi}_2$ composite's total weight gain ($< 20 \times 10^{-3}$ kg/m²) is least compared with other two composites.

Morphology of the oxidized surface of $(\text{Ti},\text{Cr})\text{B}_2 + 20\% \text{MoSi}_2$ samples after continuous oxidation up to 1000°C, (TGA) in oxygen are carried out by SEM [6]. $(\text{Ti}_{0.95}\text{Cr}_{0.05})\text{B}_2 + 20\% \text{MoSi}_2$ oxidized sample is showing the presence of severe cracks on the surface with thick glossy layer. Number of cracks decreased with increase in CrB_2 content of $(\text{Ti}_{0.90}\text{Cr}_{0.10})\text{B}_2 + 20\% \text{MoSi}_2$ composite. Fully protective and crack free glassy layer was seen on the surface of $(\text{Ti}_{0.85}\text{Cr}_{0.15})\text{B}_2 + 20\% \text{MoSi}_2$ composite. This indicates the effectiveness of CrB_2 content in the composite on the oxidation behavior.

Isothermal oxidation

Weight gain data obtained during isothermal oxidation at 750, 850 and 950°C as a function of time for all the composites are presented in Fig. 11b. Continuous weight gain with time is observed in all the samples and at all temperatures. However the rate of weight gain is different for different composites and temperatures. With increasing CrB_2 content, decrease in weight gain rate is observed. Comparing the weight gain between 750 and 950°C, it is noticed that weight gain increases with temperatures for

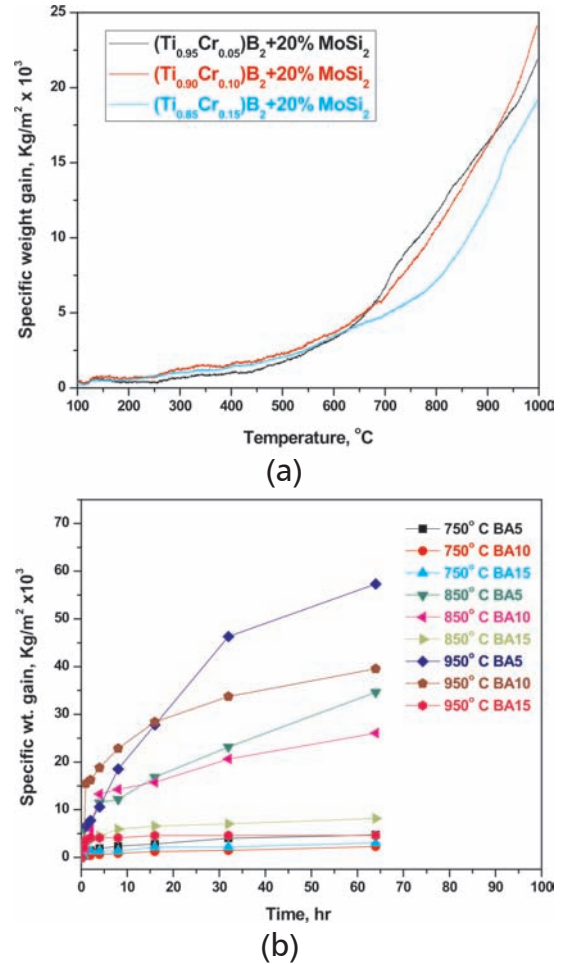


Fig. 11a) TGA plot of continuous oxidation of $(\text{Ti},\text{Cr})\text{B}_2 + 20\% \text{MoSi}_2$ composites in O_2 ; b) Specific weight gain vs. time plots of isothermal oxidation at different temperatures BA5, BA10 and BA15 represents 5, 10 and 15% CrB_2 contained composite respectively. [Reprinted from [6] with permission from Elsevier]

Table 2: Specific weight gain and rate constants after 64h of oxidation at different temperatures [Reprinted from [6] with permission from Elsevier]

Sample	Sp.wt. gain, Kg/m ² x 10 ³	Kp* (Kg ² m ⁻⁴ s ⁻¹)	Km ⁵	m [#]
At 750°C				
$(\text{Ti}_{0.95}\text{Cr}_{0.05})\text{B}_2 + 20\% \text{MoSi}_2$	4.73	1.25×10^{-10}	2.69×10^{-12}	2.687
$(\text{Ti}_{0.90}\text{Cr}_{0.10})\text{B}_2 + 20\% \text{MoSi}_2$	2.32	2.32×10^{-11}	8.50×10^{-12}	2.156
$(\text{Ti}_{0.85}\text{Cr}_{0.15})\text{B}_2 + 20\% \text{MoSi}_2$	3.06	5.26×10^{-11}	3.49×10^{-15}	3.590
At 850°C				
$(\text{Ti}_{0.95}\text{Cr}_{0.05})\text{B}_2 + 20\% \text{MoSi}_2$	34.62	5.24×10^{-9}	1.55×10^{-9}	2.327
$(\text{Ti}_{0.90}\text{Cr}_{0.10})\text{B}_2 + 20\% \text{MoSi}_2$	26.07	3.72×10^{-9}	3.57×10^{-10}	2.602
$(\text{Ti}_{0.85}\text{Cr}_{0.15})\text{B}_2 + 20\% \text{MoSi}_2$	8.17	1.75×10^{-9}	6.80×10^{-14}	4.359
At 950°C				
$(\text{Ti}_{0.95}\text{Cr}_{0.05})\text{B}_2 + 20\% \text{MoSi}_2$	57.32	1.46×10^{-8}	2.69×10^{-8}	1.807
$(\text{Ti}_{0.90}\text{Cr}_{0.10})\text{B}_2 + 20\% \text{MoSi}_2$	39.58	9.96×10^{-9}	8.01×10^{-11}	3.410
$(\text{Ti}_{0.85}\text{Cr}_{0.15})\text{B}_2 + 20\% \text{MoSi}_2$	4.58	2.14×10^{-10}	2.43×10^{-31}	10.953

(*K_p – Parabolic rate constant, ⁵K_m – Rate constant of general rate equation, #m- Slope of general rate equation)

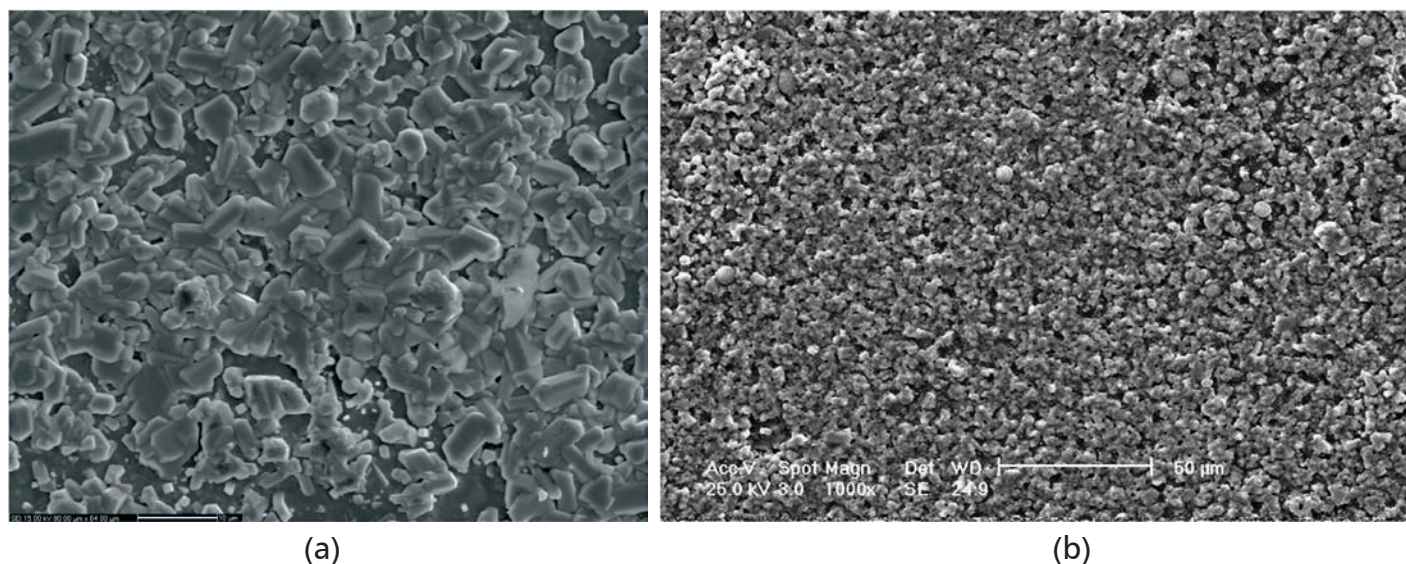


Fig.12: Morphology of the oxidized surfaces of $(\text{Ti}_{0.85}\text{Cr}_{0.15})\text{B}_2 + 20\% \text{MoSi}_2$ composites after isothermal oxidation at a) 850°C and b) 950°C for 64h in air [Reprinted from [6] with permission from Elsevier]

all the composites. But at 950°C a low specific weight gain was observed for 15% CrB_2 composites compared to that oxidized at 850°C.

In order to understand the nature of oxidation, the oxidation data was fitted in the general rate equation and parabolic law. Rate constants (K_m and K_p) and slope (m) values at different temperatures are presented in Table 2. The nature of oxidation appears to be complete parabolic ($m=2.1$ to 2.6) for 5 and 10% CrB_2 composites and cubic ($m>3$) for 15% CrB_2 composite at 750°C. One order higher parabolic rate constants are measured for the same composites at 850°C in the range of 3 to $5 \times 10^{-9} \text{ Kg m}^{-4} \text{ s}^{-1}$. The above parabolic rate constant values at 750 and 850°C indicate that mechanism of oxidation is diffusion controlled. The value of parabolic rate constant is found to decrease with increase of CrB_2 content from 5 to 15%, indicating the effectiveness of CrB_2 addition in improving the oxidation resistance.

XRD patterns of surface layer of all the composites oxidized at 750, 850 and 950°C for 64 hours are carried out. TiO_2 , Cr_2O_3 and SiO_2 phases were identified in all the composites after oxidation at 750 and 850°C. TiO_2 , CrO_3 , $\text{B}_2\text{-SiO}_5$ phases were identified in all the composites after oxidation at 950°C.

This indicates that interaction of B_2O_3 and SiO_2 resulting in the formation of a protective $\text{B}_2\text{-SiO}_5$ (eutectic mixture of $\text{B}_2\text{O}_3 + \text{SiO}_2$) phase [6].

SEM images of oxidized surfaces of all composites (5, 10 and 15% CrB_2) at 750, 850 and 950°C for 64h are also carried out. Presence of liquid phase on the surface of $(\text{Ti}_{0.85}\text{Cr}_{0.15})\text{B}_2 + 20\% \text{MoSi}_2$ composite was seen (Fig. 12a&b). At 850°C, surface cracks were not seen on the oxidized sample (Fig.12a). At 950°C, more continuous and protective oxide layer was seen (Fig.12b).

To understand the role of various elements during oxidation of $(\text{Ti}_{0.85}\text{Cr}_{0.15})\text{B}_2 + 20\% \text{MoSi}_2$ composite, extended oxidation was carried out at 850°C for 256h. Cross section of the 15% CrB_2 contained $(\text{Ti,Cr})\text{B}_2 + 20\% \text{MoSi}_2$ oxidized surface after 256h was characterized by SEM-EDS and is presented in Fig.13. The thickness of the oxide layer is $<10 \mu\text{m}$ and the elemental distribution of this layer for Si, Ti, B, Mo, Cr and O is also presented. Outer most layer of oxidized surface is seen to be that of silicon oxide. Only in the top layer of upto $10 \mu\text{m}$, there is a deficiency of the metallic elements. This layer is dominated by silicon and oxygen, clearly indicating the migration of silicon towards the outer surface [6].

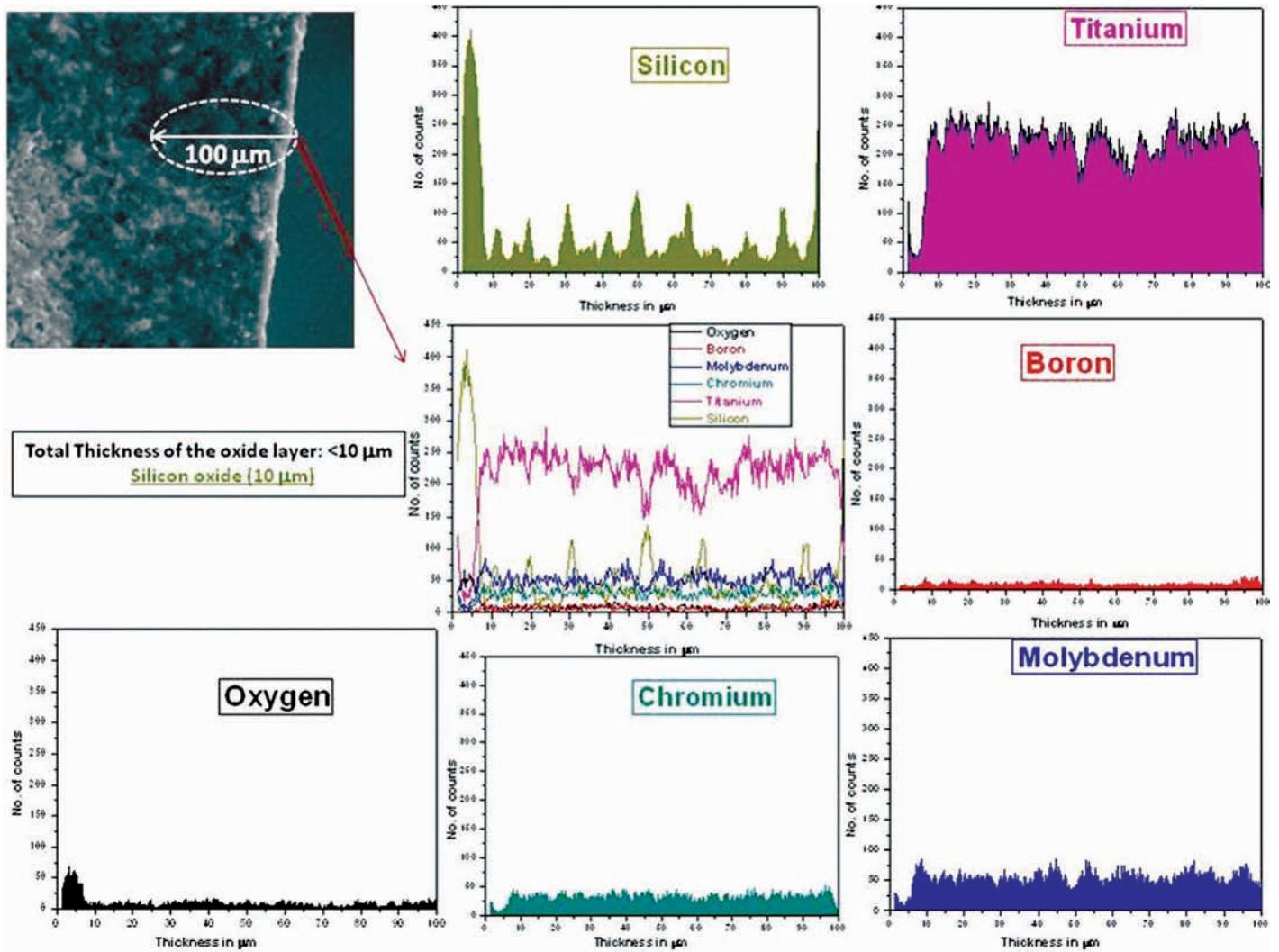


Fig. 13 Cross section of $(Ti_{0.85}Cr_{0.15})B_2 + 20\% MoSi_2$ oxidized surface after 256h at 850°C [Reprinted from [6] with permission from Elsevier]

Conclusions

1. High dense composites (4.81 g/cc) of pre-alloyed (Ti,Cr) $B_2 + 20\% MoSi_2$ were prepared.
2. Moderate hardness in the range of 24- 27 GPa and fracture toughness values in the range of 3-5 $MPa \cdot m^{1/2}$ were recorded.
3. With increased CrB_2 (5 to 15%) content, failure of this composite was found to change from predominantly transgranular to mixed (trans and intergranular) mode.
4. The nature of oxidation of the composite changed from parabolic to cubic with increase of CrB_2 content from 5 to 15%.
5. Protective oxide layers of TiO_2 , Cr_2O_3 and SiO_2 were identified on the surface of the oxidized samples at 750 and 850° C. B_2-SiO_5 phase was identified instead of SiO_2 when oxidized at 950° C.

Acknowledgements

Authors would like to acknowledge contributions of Dr. A.K.Suri, Dr. R.C.Hubli, Sri R.K.Fotedar and Sri C. Subramanian during the initial stages of this developmental activity. Support and services received from various divisions of BARC namely Material Science, Powder Metallurgy, Post Irradiation Examination, Radio Metallurgy, Analytical Chemistry, Centre for Design and Manufacturing and Laser and Plasma Technology are gratefully acknowledged.

References

1. A. K. Suri, C. Subramanian, J. K. Sonber and T. S. R. Ch. Murthy; "Synthesis and consolidation of boron carbide: A Review"; (Full critical review) International Materials Review, 55[1], (2010) 4-40
2. B. Basu, G.B. Raju, and A.K. Suri; "Processing and

- properties of monolithic TiB_2 based materials", International Materials Reviews 51[6] (2006) 354-74
3. K. Sairam, J.K. Sonber, T.S.R.Ch. Murthy, C. Subramanian, R.K. Fotedar, R.C. Hubli, "Reaction Spark Plasma Sintering of Niobium diboride", Int. J. Refract. Met. Hard Mater. 43, (2014) 259-262
 4. J.K. Sonber K. Sairam, T.S.R.Ch. Murthy, A. Nagraj, C. Subramanian and R.C. Hubli; "Synthesis, densification and oxidation study of lanthanum hexaboride", J European Ceramic Society 34, (2014) 1155-1160
 5. R.D. Bedse, J. K. Sonber, K. Sairam, T.S.R.Ch. Murthy, R. C. Hubli; "Processing and characterization of CrB_2 based novel composites" , High Temperature Materials and Processes (HTMP) (2015) (Accepted) DOI: 10.1515/htmp-2014-0084, January 2015
 6. T.S.R.Ch. Murthy, J.K. Sonber, C. Subramanian, R.C.Hubli N. Krishnamurthy and A.K. Suri, "Densification, characterization and oxidation studies of $(Ti,Cr) B_2+20\%MoSi_2$," Int. J. Refract. Met. Hard Mater. 37, (2013) 12-28
 7. T.S.R.Ch. Murthy, J.K. Sonber, C. Subramanian, R.C. Hubli N.Krishnamurthy and A.K.Suri, "Densification and Oxidation behavior of a novel $TiB_2 - MoSi_2 - CrB_2$ composite" Int. J. Refract. Met. Hard Mater. 36, (2013) 243-253
 8. J.K. Sonber, T. S. R. Ch. Murthy, C.Subramanian, R. C. Hubli and A. K. Suri; "Synthesis, densification and characterization of EuB_6 ", Int. J. Refract. Met. Hard Mater. 38, (2013) 67-72
 9. T.S.R.Ch. Murthy, J.K. Sonber, C. Subramanian, R.C. Hubli and A.K. Suri, "Densification, Characterization and Oxidation studies of $TiB_2 + WSi_2$ composite" Int. J. Refract. Met. Hard Mater. 33, (2012) 10-21
 10. J. K. Sonber, T. S. R. Ch. Murthy, C. Subramanian, Sunil Kumar, R. K. Fotedar and A.K. Suri "Investigations on synthesis of ZrB_2 and development of new composites with HfB_2 and $TiSi_2$ ", Int. J. Refract. Met. Hard Mater. 29, (2011) 21-30
 11. T.S.R.Ch. Murthy, J.K. Sonber, C. Subramanian, R.K. Fotedar, S. Kumar, M.R. Gonal and A.K. Suri, "A New $TiB_2 + CrSi_2$ composite - Densification, Characterization and oxidation studies" Int. J. Refract. Met. Hard Mater. 28, (2010) 529-540
 12. T.S.R.Ch. Murthy, C. Subramanian, R.K. Fotedar, M.R. Gonal, P. Sengupta, S. Kumar, A. K. Suri "Preparation and property evaluation of TiB_2+TiSi_2 composite" Int. J. Refract. Met. Hard Mater. 27, (2009) 629-636
 13. T.S.R.Ch. Murthy, J.K. Sonber, C. Subramanian, R.K. Fotedar, M.R. Gonal and A.K. Suri; "Effect of CrB_2 addition on densification, properties and oxidation resistance of TiB_2 ", Int. J. Refract. Met. Hard Mater. 27[6], (2009) 976-984
 14. J. K. Sonber, T. S. R. Ch. Murthy, C. Subramanian, S. Kumar, R. K. Fotedar and A. K. Suri, "Investigation on synthesis, pressureless sintering and hot pressing of chromium diboride"; Int. J. Refract. Met. Hard Mater. 27, (2009) 912-918
 15. C.Subramanian, T.S.R.Ch.Murthy, A. K. Suri, "Synthesis and consolidation of titanium diboride"; Int. J. Refract. Met. Hard Mater. 25 (2007) 345-350
 16. G.R. Anstis, P. Chantikul, B.R. Lawn, D.B. Marshall, "A critical evaluation of indentation techniques for measuring fracture toughness: I, direct crack measurements"; J. Am. Ceram. Soc. 64 (1981) 533-538.

Design of Sealing Arrangements for Development of Leak Tight Articulated Manipulator For Waste Management and Reprocessing Plants

Satish B. Patil and Avinash K. Mudaiya
Technology Development Division

Abstract:

As a part of development of Remote handling equipment and gadgets, Leak tight Articulated Manipulator (ARTM) has been developed for shielded facilities of Nuclear Recycle Plant. The ARTM is a Master Slave Manipulator having 8 Kg Payload capacity and most suitable for shielded sampling cubicles of Waste Management plants and dilution hot cells of Reprocessing plants. All the motions and forces are transmitted from Master to slave arm through the mechanical linkages, which are housed inside the wall tube. The mechanical linkages and wall tube run across the shielded wall. The applications involving seal tightness of the glove boxes and dilution hot cells intend to use all the accessories including MSMs to be leak tight. During the design of leak tight ARTM, all the potential leak paths through the components of existing ARTM were examined critically and static and dynamic seals were designed based on the geometry and requirement of particular leak path. A leak proof testing set up was fabricated for evaluating the leak rates across the manipulator contemplating the actual operating conditions. The manipulator was subjected to the Friction, Rigidity and Leak tests. The results of the tests are satisfactory and as per the International standards available. The leak rates measured for different manipulators were in the range of 0.05 to 0.1 % of air volume/hr @ 200 mm of water column differential negative pressure.

Introduction

Remote handling is very important aspect of the radioactive waste management and Reprocessing Plants. Master Slave Manipulators (MSM) were developed to carry out the material handling and maintenance activities inside a radioactive hot cell. Master arm of the MSM remains outside of the hot cell while slave arm is inside the hot cell. All the motions and forces are transmitted from Master to slave arm through the mechanical linkages, which are housed inside the wall tube. The mechanical linkages and wall tube run across the thick shielded walls. The applications involving seal tightness of the glove boxes and dilution hot cells intend to use all the accessories including MSMs to be leak tight.

During development all the leak paths were examined very critically. The critical leak paths were analyzed in order to design the components so that leaks across the boundary shielding wall will be reduced to minimum possible. The static seals and dynamic seals have been provided to facilitate leak tightness ensuring the free motion of the moving components. The collapsible flexible bellows have been provided for sealing the motion transmission rods across the wall tube. The protective bootings have also been developed for the slave arm which will serve as a secondary leak tight barrier for the manipulator. The manipulators have

been manufactured and subjected to different tests mainly Friction, Rigidity and Leak tightness as per the technical specifications, endorsed by the end users. This paper explores design aspects of leak tight Articulated manipulator, testing procedure, acceptance criteria and the actual results of the developmental work.[1][2]

Objective

The objective of the developmental work was to achieve leak tightness, across the manipulator, of the order of 0.1 % of air volume/hr @ 200 mm of water column differential pressure.

Design Concept

Potential Leak Paths

Initially the potential leak paths were examined for the assembly of the Articulated Manipulator components as shown in Fig. 1. The necessary static seals (O-rings and gaskets) for stationary parts and dynamic seals for rotary parts were designed for arresting the leakages from the leak paths. Necessary flange designs were also modified to accommodate the required seals. After manufacturing of the individual components with provisions of the seats for seals, all the seals were fitted and the assembly was tested for the leak rates. In addition to the static and dynamic seals,

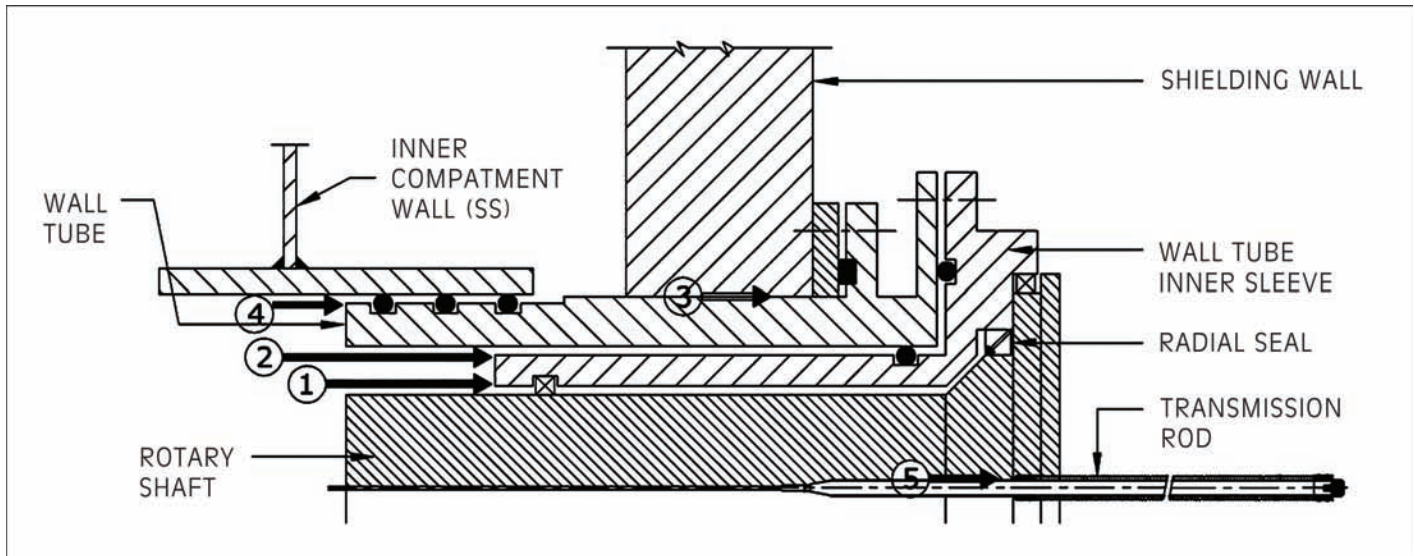


Fig. 1: Pictorial view of potential Leak Paths

a leak tight Polyurethane booting was also provided as an additional barrier for arresting the leakages. Following are the leak paths across the manipulator wall:

- 1) Leak path through wall tube assembly,
- 2) Leak path through wall tube and sleeve,
- 3) Leak path through wall tube sleeve and embedded Pipe,
- 4) Leak path between sleeve and Inner compartment wall,
- 5) Leak path along the transmission rods.

Static Seals

To prevent the leakage of air through the leaking paths which are operating in static condition the O Rings have been provided. The main advantages of the O rings as static seals are sealing over large range of pressure, temperature and tolerances. Ease of service and no critical torque requirement for tightening, causing structural damage, are the main features of O-ring seals. The O-rings occupy less space, they are light in weight and facilitates the gradual identifiable failure during operation. Ethylene Propylene Dien Rubber (EPDM) material withstanding upto 150° C and having 50 MRad radiation resistance was selected for the O-rings. [3] While selecting the O-rings, selection criteria such as Wear test, Aging test, Coefficient of thermal expansion, Compression set, Hardness, Tensile strength, Elongation and Radiation resistance was laid down.

Dynamic Seals

Dynamic seal has been selected to achieve the design goals such as to prevent leakage at outer diameter, to avoid rotation or coming out of the bore, compatible with

the bore material, easy to install, to compensate for bore imperfections and to be suited for automated installation. Following parameters were used for selection of appropriate seal from the Simrit radial seal catalogue [4]

- a) The general category of the seal application.
- b) Operating conditions like Shaft Speed, Pressure and Eccentricity
- c) Appropriate lip, case and spring material.
- d) Bore and shaft configurations to ensure compatibility with seal.

During designing the components, guidelines given in the product catalogue were used for the shaft and housing features of the dynamic seals.

Sealing Aspects for Sealing Surfaces

Seal and shaft compatibility is dependent on shaft tolerance, lead-in chamfer, finish and hardness. Proper consideration of these conditions will assist in providing optimal seal performance. Hardness of shaft is an important factor to prevent excessive wear, deformation, scratches, and to allow for easy machining for appropriate roughness value. Under normal conditions, the seal contact area of the shaft has been maintained with hardness of Rockwell C45.

Shaft surface roughness is very important as it greatly influences the amount of lip wear. The roughness of the shaft surface should be in the range of 0.25 μM to 0.50 μM Ra and Rmax in the range of 0.8 - 3.2 μM . A shaft chamfer has been provided to assist in the installation process.

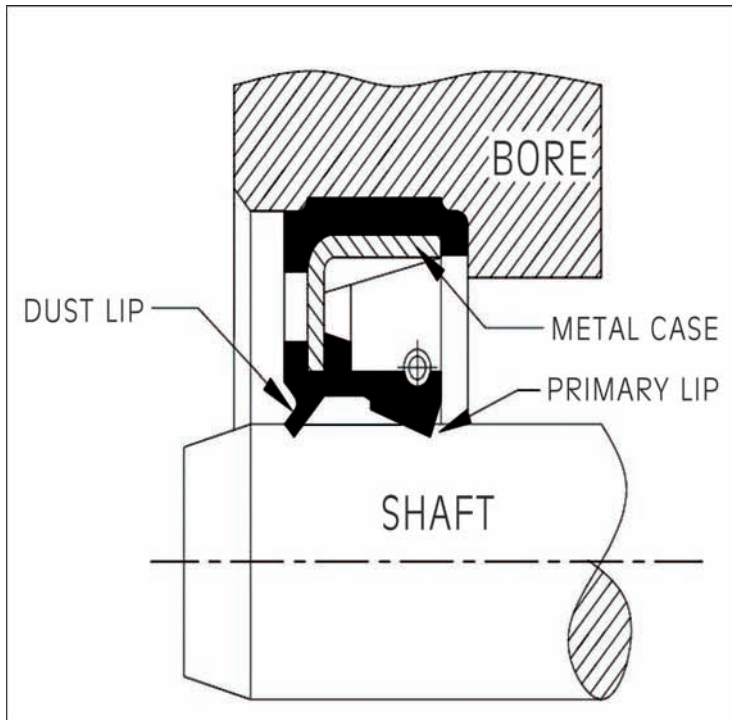


Fig. 2: Installation of Dynamic seal

Without a proper chamfer, the seal lip may get damaged or distorted resulting in a dislodged garter spring. [4]. A bore chamfer is necessary to assist in installation of the seal.

Leak Testing of Articulated Manipulator

A leak test setup comprising of a cylindrical seamless tube, which can accommodate the entire slave arm in straight condition was fabricated as shown in Fig. 3 & 4. A vacuum equivalent to 200 mm of water column was generated by using a positive displacement vacuum

pump. Initially the test set up was qualified for the leak tightness.

During assembly of ARTM, the wall tube assembly equipped with the components like motion transmitting rod bellows and dynamic radial seal were tested for leak rates if any as shown in Fig. 3. In case of leakage, the corrective action like replacement of faulty component was taken to overcome the leakage. After getting assurance of the leak tightness of these individual components the entire assembly of the articulated manipulator was carried



Fig. 3: Leak testing of Individual Component

out and leak testing was continued for the period of 8 hours.

Evaluation of Leak Rates

The manipulator was installed in a leak tight dilution hot cell similarly as shown in Fig. 6 for measurement of the leak rates across the manipulator wall tube. The dilution hot cell was subjected to negative pressure equivalent to 200 mm of water column. The pressures and temperatures were allowed to get stabilized before recording the initial readings. The Pressure and temperature readings were recorded after 30 minutes interval for entire test duration of 8 hours. The Leak rate in terms of % of air volume/hr @ 200 mm of water column differential pressure was calculated by using the formula:

$$\% \text{ Leak Rate} = [(P_1 \times T_2) / (P_2 \times T_1) - 1] \times (1/t) \times 100$$

Where, P_1 = Initial pressure (absolute) inside the test chamber

T_1 = Initial temperature inside the test chamber

P_2 = Final pressure (absolute) inside the test chamber after time 't' hrs

T_2 = Final temperature inside the test chamber after time 't' hrs

P_0 = Atmospheric pressure

T_0 = Atmospheric temperature

Slave Arm Protective Bootings:

Slave arm of the Articulated Manipulator has been provided with Polyurethane booting for protecting it from the



Fig. 4: Actual set up for Leak testing

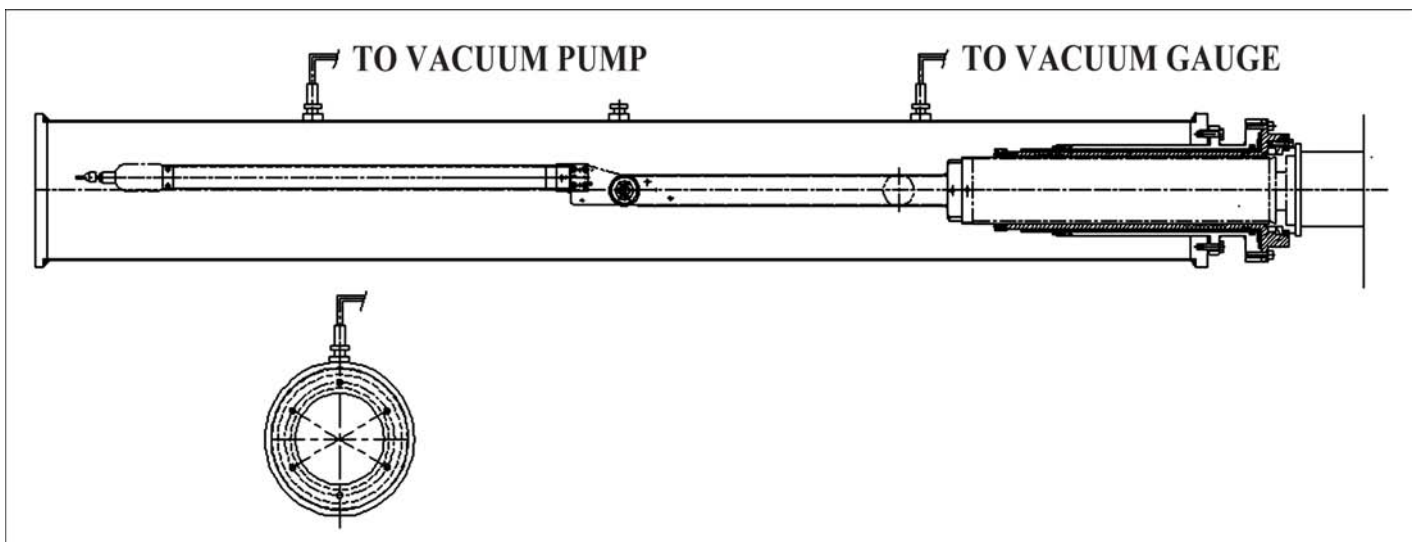


Fig. 5: Set up for Leak Testing

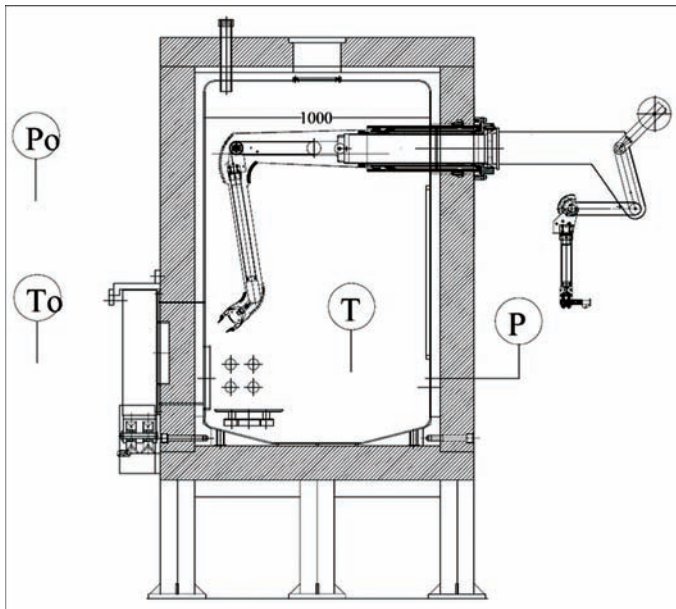


Fig. 6: Installation of Articulated Manipulator in Dilution Hot Cell

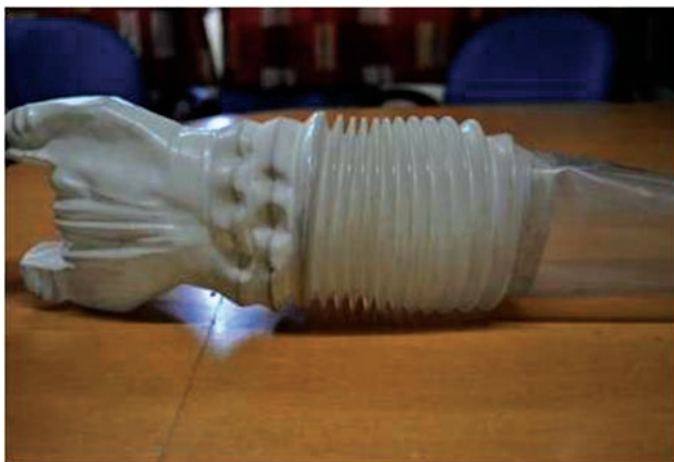


Fig. 7: Slave Arm Booting

deposition of radioactive contamination as shown in Fig. 7. The slave arm booting also provides the secondary barrier against the leakage. However to be on the conservative side the slave arm booting has not been considered during evaluation of the leak rates across the manipulator.

The Polyurethane bootings have been indigenously developed for Articulated Manipulators. For manufacturing this product the aluminum dies have been fabricated with the convolutions on cylinder. Different types of dies have been manufactured for different portion of the booting. The appropriate radius is provided on the edges of the convolutions to avoid the sharp edges. The PU Solution is prepared in a vertical container at uniform temperature and the die is lowered into the container, kept for sufficient time so that the uniform layer of

PU forms on the die. The die is removed from the container and allowed to dry. The thickness of the layer is measured and same sequence of operation is repeated till the required thickness of the layer is achieved. Non-collapsible Booting Section for overhang and fixed length up to the elbow joint made from 0.5 mm thick PU sheet.

Collapsible PU Booting Section for the telescopic section formed by layers of PU Casting on a special aluminum alloy die in following steps.

- i) Compounding, stock mix preparation and maturation
- ii) Segment casting & Curing
- iii) The collapsible and non-collapsible sections are stitched together by using adhesives and high frequency welding process.

After manufacturing the bootings are inspected to verify the conformance of the booting to the specifications. An elaborate test set up for the inspection of booting has been prepared. All the bootings are subjected to

- a) Dimensional check.
- b) Leak test- the booting is tested for leakage by the soap bubble test against gauge pressure of 8" of water column applied internally.
- c) Pull Out test - the booting material joints is subjected to a tensile test in order to check joint strength of the stitch which is around 65 Kg/in².
- d) Periodic irradiation of the sample to verify its resistance to accumulated dose of 100 MRad.

Testing of Articulated Manipulators

The deployment of static and dynamic seals for achieving the leak tightness of the manipulator affects the smoothness of the operation and frictional losses in most of the joint motions. However the optimum limiting values of the frictional losses have been determined based on which the manipulators are finally qualified for the operation. Following tests are required to be carried out on manipulator during final testing and inspection:

- a) Dimensional Check
- b) Arm Reach Test
- c) Friction Test for all motions
- d) Rigidity Test
- e) Load Test
- f) Leak Tightness Test



Fig. 8: Leak Tight Articulated Manipulators in Operation at PRTRF Lab

Installation & Commissioning at PRTRF Lab

Twelve arms of Leak Tight Articulated Manipulators have been recently installed and commissioned at Uranium separation lab of PRTRF plant, Trombay. All the manipulators have performed satisfactorily during the active run of the PRTRF Plant. Fig. 8 shows the actual photograph of the Articulated Manipulators in operation at PRTRF, Trombay.

Conclusion

Leak tight version of Articulated Manipulator has been developed successfully. The manipulator was subjected to the Friction, Rigidity and Leak tests. The results of the tests were satisfactory as per the International standards available. The leak rates measured for different manipulators were in the range of 0.05 to 0.1 % of air volume/hr @ 200 mm of water column differential negative pressure.

Acknowledgement

The authors are grateful to Shri K.K. Prasad, Shri R.K. Gupta, Shri K.N.S. Nair, Shri S.S. Khan and Shri Sandesh Mohite for their invaluable technical support. We are also thankful to M/s HMT Machine Tools Ltd., Bangalore and M/s IRMRA, Thane for manufacturing and testing support.

References

1. International Standard, ISO 10648-2, 1994, Containment enclosures Part-2, Classification according to leak tightness and associated checking methods.
2. ASTM C 852-93, Standard guide for Design Criteria for Plutonium Glove Boxes.
3. Parker O- Ring Handbook, ORD 5700
4. Simrit Seals, Radial Shaft seal catalogue - 2008

Design and screening of extractants for Zr⁴⁺-Hf⁴⁺ separation: Synergistic approach using molecular modelling and solvent extraction

Sk. Musharaf Ali, A. Boda, G. Pandey, S. Mukhopadhyay and K.T. Shenoy

Chemical Engineering Division

and

R. Singh, M. Paramanik and S.K.Ghosh

Bio-Organic Division

Abstract:

The preferential selectivity of Zr⁴⁺ over Hf⁴⁺ ion towards mixed alkyl organophosphorus extractants is predicted using molecular modelling and solvent extraction studies. Density Functional theory successfully captures the higher complexation stability of mixed alkyl phosphine oxide (MAPO) over mixed alkyl substituted phosphine oxide (MSAPO) for both Zr⁴⁺ and Hf⁴⁺ ions as observed in the solvent extraction experiment. Further, the extraction energy for Zr⁴⁺ ion is higher than Hf⁴⁺ ion with MAPO over MSAPO. The calculated extraction energy follows the same order of distribution constant as predicted by the solvent extraction which shows that MAPO is the best extractant in terms of higher distribution constant and selectivity over MSAPO.

Introduction

Zirconium and Hafnium co-exist in nature and due to their similar chemical properties (ionic diameter of Zr⁴⁺ and Hf⁴⁺ is 1.54 and 1.52 Å respectively); they are commonly referred to as chemical isotopes. However, these metals have opposite nuclear characteristics. Zr is used in nuclear reactors as structural material and Hf having high neutron absorption cross section, is used as a control material in water-cooled nuclear reactors. It is important to separate Zr⁴⁺ and Hf⁴⁺ prior to their transformation into pure metals due to their different use in nuclear industry [1]. Because of their similar chemical properties, it is very difficult and hence challenging to separate them from their aqueous solution.

Different organophosphorous ligands such as TBP, trialkylphosphine oxide (TOPO), its branched chain analogue (Cyanex) and many more have been employed in the solvent extraction studies of Zr⁴⁺ and Hf⁴⁺ [2-10]. Solvent extraction processes are currently employed on a commercial scale to separate Hf⁴⁺ from Zr⁴⁺ ions using tri-n-butyl phosphate (TBP) as extractant with kerosene as diluents [2, 11]. The major negative aspect of the TBP process is the low separation factor (SF=D_{Zr}/D_{Hf}=10, where D is distribution constant) and third phase formation. There is a continuing search for finding superior ligands than TBP. Recently, ligands of Cyanex family (bis(2,4,4-trimethylpentyl) octyl phosphine oxide) have been shown to be a better extractant for Zr⁴⁺ ion separation compared to the much practiced TBP [12]. The experimental separation factor of Zr/Hf with TBP was found to be 10, whereas it was 40 with ligands of

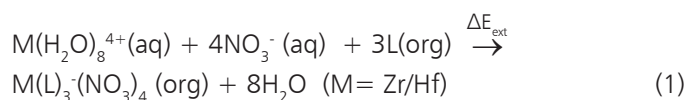
Cyanex family. The selectivity between two class of ligands was 4. Therefore, we have undertaken to model the ligands of Cyanex family for the extraction of Zr⁴⁺/Hf⁴⁺ to explore the underlying extraction mechanism by studying the ion-ligand interaction through density functional electronic structure calculation. The theoretical understanding on the interaction of the Zr⁴⁺-Hf⁴⁺ ions with organophosphorus ligands using quantum chemical calculation is very limited. Recently, we have reported the higher selectivity of ZrO²⁺ over HfO²⁺ oxycation towards TBP using electronic energy calculation [13]. However, so far as we know, no theoretical investigation has been reported about the selectivity of mixed alkyl phosphine oxide ligands with Zr⁴⁺ and Hf⁴⁺ metal cations in spite of their enormous role in nuclear technology. Hence, it is of very much desirable to focus on the Quantum chemical study on the selectivity of Zr⁴⁺-Hf⁴⁺ to deliver a suitable ligand/solvent system for efficient separation of Zr⁴⁺ from Zr⁴⁺-Hf⁴⁺ mixtures. Therefore, our systems of interest are alkyl phosphine oxide (MAPO) and mixed substituted alkyl phosphine oxide (MSAPO). The structures and energetic parameters for the free ligand, hydrated metal ion and the metal-ion-ligand systems were computed using DFT [14]. Conductor like screening model (COSMO) solvation approach was used to account for the solvent effect in water-organic bi-phasic system.

Computational methodology

Bis (hexy)-octyl phosphine oxide and (bis(2,4,4-trimethylpentyl) octyl phosphine oxide) are the major constituting species in the composition of MAPO and

MSAPO. Hence, minimum energy structure of bis (hexyl)-octyl phosphine oxide (MAPO) and bis (2, 4, 4-trimethylpentyl) octylphosphine oxide (MSAPO) and their complexes with Zr^{4+} and Hf^{4+} ions were optimized with generalized gradient approximation based BP86 functional employing split valence valence plus polarization (SVP) basis set as implemented in Turbomole package [15]. Effective core potential (ECP) was used for both Zr and Hf where 28 and 60 electrons are kept in the core of Zr and Hf respectively [16]. BP86 functional consists of Becke B88 exchange functional [17] and Perdew P86 correlation functional [18] and was found to be successful in predicting various molecular properties. The free MAPO and MSAPO ligands and their complexes with metal ions were optimized without imposing any symmetry restriction.

The selectivity of one metal ion over another can be predicted using extraction energy (ΔE_{ext}). The metal ion-ligand complexation reaction is modeled as the 1:3 ($M^{4+}:3L$) stoichiometric reaction as follows.



Here L corresponds to either MAPO or MSAPO ligands. The 1:3 ($M^{4+}:3L$) stoichiometric reaction was reported from solvent extraction study.

GGA based BP86 has the inbuilt limitation in the accurate energy predictions due to non-consideration of non-covalent interaction. Hence, single point energy calculation was further performed using BP86 optimized structures at B3LYP level of theory [19], which was known for its theoretical accuracy over simple GGA functional. The extraction energy is calculated as

$$E_{ext} = E_{M(NO_3)_4 \cdot 3L(org)} - (E_{M^{4+}(H_2O)_8(aq)} + 3E_{L(org)} + 4E_{NO_3^-(aq)}) \quad (2)$$

Most of the metal ion extraction takes place from the aqueous solution phase to the organic solvent phase aided by the ligand. Hence, the consideration of solvent effect on the complexation of the ligand moiety with metal ion in the QM calculation is thus indispensable. In order to study the aqueous and organic solvent effect, the optimized geometry obtained from BP86 level of theory was used for single point energy calculation using conductor like screening model (COSMO) [20] as implemented in TURBOMOLE quantum chemistry package. The dielectric constant, ϵ of water and dodecane was taken as 80 and 2 respectively. The MOLDEN

graphical program [21] was used for the visualization of various molecular geometry and structural parameters.

Results and Discussion

Computational

Structural parameters

Mostly metal ions are extracted from the aqueous environment, hence, hydrated Zr^{4+} and Hf^{4+} are optimized first and their structures are presented in Fig.1.

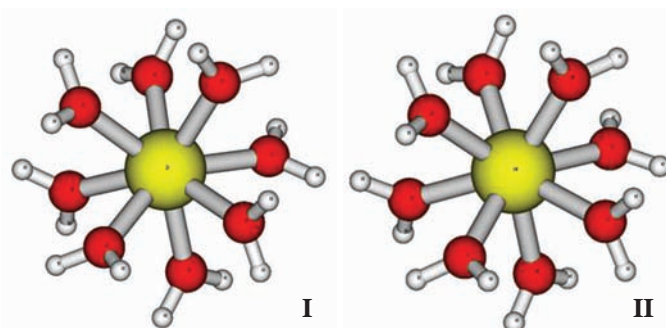


Fig. 1. Optimized structures of hydrated (I) $Zr^{4+}(H_2O)_8$ and (II) $Hf^{4+}(H_2O)_8$ complexes

Both Zr^{4+} and Hf^{4+} ions are shown to be octa coordinated with Zr-O and Hf-O bond distance of 2.272Å and 2.270Å respectively. The very close distance of Zr^{4+} and Hf^{4+} ions in the hydrated cluster is reflected in their similar chemical properties and thus poses a great challenge for their mutual separation. The computed minimum energy structures of free extractants are displayed in Fig.2. The P=O bond distance of MAPO and MSAPO was found to be 1.524Å and 1.525Å respectively. The optimized structures of complexes of Zr^{4+} and Hf^{4+} ions towards MAPO and MSAPO are presented in

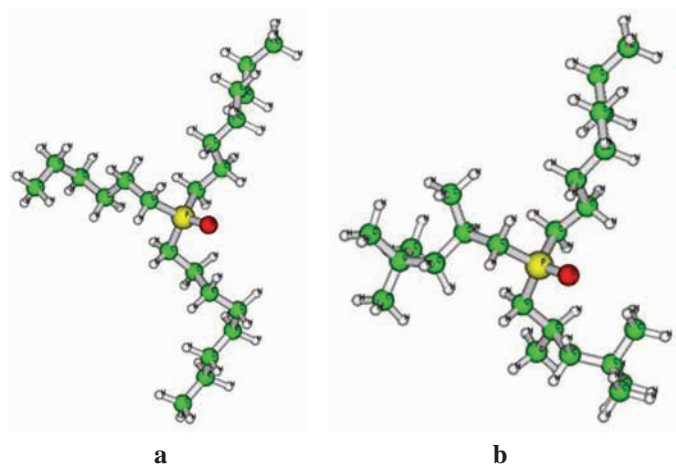


Fig. 2: Optimized structures of (a) MAPO and (b) MSAPO

Fig.3. From figure 3 it is seen that both Zr^{4+} and Hf^{4+} ions are coordinated to the 4 nitrate ions and three extractants. Three nitrate ions are coordinated in mono-dentate fashion and one nitrate ion in bidentate fashion leading to eight coordination complex.

The calculated structural parameters of the metal ion complexes are presented in Table.1. From the table it is seen that the M-O (phosphonic O) bond distance is shorter than that of M-O (O of Nitrate) bond distance indicates the stronger interaction with phosphine "O" atom. Further, the M-O bond distance for mono-dentate nitrate is shorter than that of bi-dentate nitrate ion.

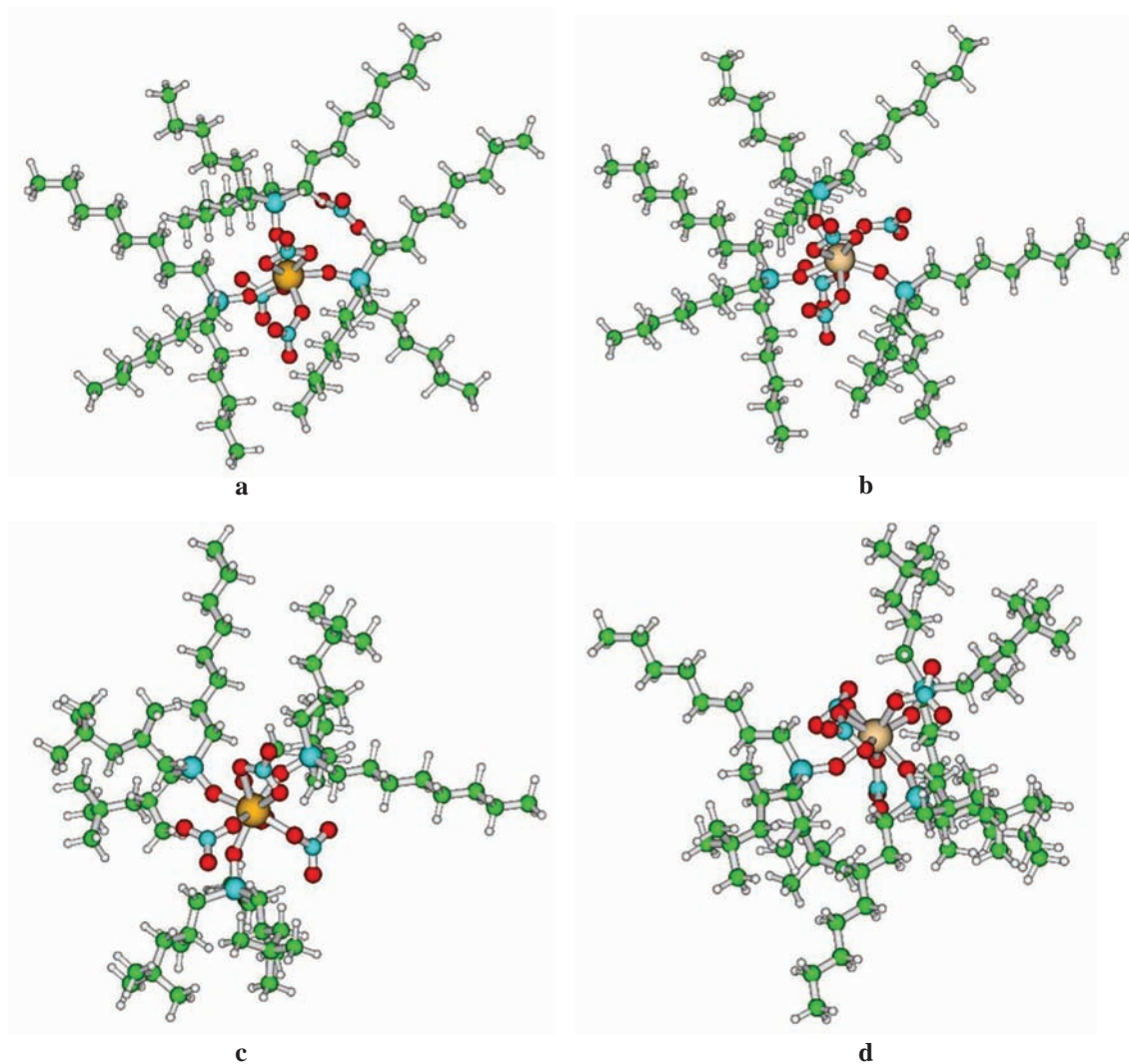


Fig. 3: Optimized structures of nitrate complex of Zr and Hf with different extractants: (a) $Zr(NO_3)_4-(MAPO)_3$ (b) $Hf(NO_3)_4-(MAPO)_3$ (c) $Zr(NO_3)_4-(MSAPO)_3$ and (d) $Hf(NO_3)_4-(MSAPO)_3$. The green, cyan, red and grey sphere represents the C, N, O and H atom respectively. The dense and light yellow sphere represents Zr and Hf atom respectively.

Table 1: Calculated structural parameters (Å) of nitrate complexes of Zr /Hf with MAPO and MSAPO.

System	Zr			Hf		
	Zr-O (phosphonic O)	Zr-O (O of NO_3)		Hf-O (phosphonic O)	Hf-O (O of NO_3)	
		Mono	Bi		Mono	Bi
MSAPO	2.161	2.210	2.383	2.154	2.206	2.382
MAPO	2.092	2.138	2.340	2.166	2.204	2.345

The Zr-O and Hf-O bond distances are very close to each other suggesting their similar interaction towards the ligands. After complexation with Zr^{4+} and Hf^{4+} ions, the P=O bond distance was found to be elongated for both MAPO and MSAPO. The P=O bond distance in MSAPO was changed to 1.565Å and 1.564Å after complexation with Zr^{4+} and Hf^{4+} ions respectively, whereas the P=O bond distance was found to be lengthen to 1.582Å and 1.581Å with MAPO with Zr^{4+} and Hf^{4+} ions respectively. This elongation of bond length indicates the strong interaction of phosphonic O donor and the metal ion. Further, the elongation is higher with MAPO over MSAPO suggesting higher interaction for MAPO over MSAPO.

Extraction energy

The gas phase binding energy for both Zr^{4+} and Hf ions with the MAPO and MSAPO extractants are tabulated in Table 2. The computed binding energy was found to be higher with MAPO compared to MSAPO for both Zr^{4+} and Hf^{4+} ions. Furthermore, the binding energy was found to be higher for Zr^{4+} over Hf^{4+} ion for all the extractants considered here indicates that Zr^{4+} ion will be extracted preferentially over Hf^{4+} ion in a solution.

Next, the calculation was extended to solvent phase to capture the more realistic picture. The computed extraction energy is also presented in Table 2. The computed extraction energy was found to be higher with MAPO compared to MSAPO for both Zr^{4+} and Hf^{4+} ions with higher extraction energy for Zr^{4+} over Hf^{4+} ion. The extraction energy was found to be reduced considerably compared to gas phase binding energy due to dielectric screening of the solvents. Higher extraction energy for Zr^{4+} ion over Hf^{4+} ion leads to preferential extraction of Zr^{4+} ion over Hf^{4+} ion. The theoretical separation factor can be calculated by using the relation: $SF(Zr/Hf) = \text{Exp}(-\Delta\Delta E/RT)$, where R is the universal gas constant and T is the temperature (298.15K). The calculated theoretical separation factor for Zr^{4+} and Hf^{4+} towards MAPO and MSAPO was found to be 57.23

and 41.54 respectively. The experimental separation factor was found to be 20 and 12.06 respectively. The calculated separation factor using DFT was found to be higher than that of obtained from experiments. This is because of the limitation of theory, which cannot handle the large number of molecules as well as other practical parameters like experiments. Also, the thermodynamic correction was not done to the extraction energy. Hence, in view of the limitation of the theory and the complexity of the chemical system, the theoretical values are seems to be fairly reasonable. Further, the selectivity factor for Zr^{4+} - Hf^{4+} separation between two ligands (here MAPO and MSAPO) can be evaluated using the relation: $\text{selectivity factor} = SF_{(Zr/Hf)MAPO} / SF_{(Zr/Hf)MSAPO} = \text{Exp}(-\Delta\Delta\Delta E/RT)$. The calculated theoretical value of selectivity factor was found to be 1.37 which is very close to the experimentally determined value of 1.65.

Molecular Descriptors for MAPO and MSAPO

DFT has an extra-ordinary potential for calculating global and local indices that describe the inherent reactivity of chemical species quantitatively and is thus very useful to describe the host (alkyl phosphine ligands) guest (metal ion) type interaction. Chemical systems are commonly characterized by its electronic chemical potential, μ and absolute hardness, η and are defined as [22]

$$-\mu = (I+A)/2 = \chi \quad \eta = (I-A)/2 \quad (3)$$

where I is the ionization potential and A is the electron affinity. Here, χ is called the absolute electronegativity. According to Koopmans' theorem [23], I and A can be obtained as

$$I = -E_{\text{HOMO}} \quad A = -E_{\text{LUMO}} \quad (4)$$

If donor acceptor system is brought together, electrons will flow from that of lower χ to that of higher χ , until the chemical potentials become equal. The amount of charge transfer, ηN can be calculated by applying the following formula [24]

Table 2: Calculated extraction energy of Zr and Hf⁴⁺ with MAPO and MSAPO ligands.

System	Binding energy(ΔE) (kcal/mole)				$\Delta\Delta E$ ($\Delta E_{Zr} - \Delta E_{Hf}$) (kcal/mole)	$\Delta\Delta\Delta E$ (kcal/mole)
	Gas phase		Solvent phase			
	Zr^{4+}	Hf^{4+}	Zr^{4+}	Hf^{4+}		
MSAPO	-974.30	-971.32	-81.03	-78.82	-2.21	-0.19
MAPO	-1002.00	-1000.11	-108.76	-106.36	-2.40	

$$\Delta N = (\chi_M - \chi_L) / \{2(\eta_M + \eta_L)\} \quad (5)$$

Here, M stands for metal ion, which acts as Lewis acid i.e. acceptor and L stands for MAPO or MSAPO, which acts as Lewis base i.e. donor.

A higher value of E_{HOMO} indicates a tendency of the molecule to donate electrons to appropriate acceptor molecule of low empty molecular orbital energy. On the other hand, the energy of the lowest unoccupied molecular orbital indicates the ability of the molecule to accept electrons. Larger values of the energy difference, $\Delta E = E_{LUMO} - E_{HOMO}$, provide low reactivity to a chemical species and lower values of the energy difference indicates higher reactivity.

The calculated values of HOMO-LUMO energy gap, absolute hardness (η), absolute electro negativity (χ) and charge transfer, ΔN of the optimized ligand–metal ion systems are given in Table. 3. In order to calculate the fractions of electron transferred from the donor MAPO/MSAPO to the metal ion, theoretical values for absolute electronegativity and absolute hardness for hydrated Zr^{4+} and Hf^{4+} ions were calculated. The theoretical values of absolute electronegativity of hydrated Zr^{4+} and Hf^{4+} ions are 23.11eV and 22.18eV and absolute hardness are 3.17eV and 3.52eV respectively. This indicates that Zr^{4+} metal ion is relatively hard acid compared to Hf^{4+} ion.

According to Pearson’s HSAB principle, hard acids prefer to bind to hard bases and soft acids prefer to bind to soft

bases. MAPO/MSAPO with phosphine oxygen as donor atom acts as a hard base as evident from high values of hardness (Δ) and electro negativity (χ). Hence in accordance with the HSAB principle MAPO/MSAPO prefers Zr^{4+} metal ion over Hf^{4+} metal ion during complexation. A large value of ΔN is favorable for a donor-acceptor reaction. The value of ΔN is higher for Zr^{4+} ligand system than Hf^{4+} -ligand system, which indicates that the complexation with Zr^{4+} metal ion is more favorable than Hf^{4+} metal ion.

Experiments

Two varieties of mixed alkyl phosphine oxide namely MSAPO and MAPO were synthesized in Chemical Engineering Division. Liquid–liquid extraction batch studies were performed at room temperature for various extractant concentration, to obtain $\log [\text{extractant}]$ v/s $\log [K_d]$. O/A is maintained 1:1 in all the cases. ICP-OES instrument was used for the analysis to obtain the concentration of metal ion in aqueous phase. Dodecane and isodecanol were used as diluents in 80:20 ratio. The metal ion extractant stoichiometry was determined by plotting distribution constant versus concentration of the MAPO extractant as displayed in Fig. 4.

For MAPO, the stoichiometry was 1:3 for both Zr^{4+} and Hf^{4+} ions, whereas for MSAPO, it was 1:3 for Zr^{4+} ion and 1:2 for Hf^{4+} ion. The experimentally determined K_d values for MAPO and MSAPO are presented in Table 3.

Table.3: Molecular descriptors for Zr^{4+} and Hf^{4+} ions with MAPO and MSAPO ligands.

System	ΔE (eV) (HOMO-LUMO)	χ (eV)	η (eV)	ΔN	
				MSAPO	MAPO
$Zr^{4+}-(H_2O)_8$	6.33	23.11	3.17	1.493	1.481
$Hf^{4+}-(H_2O)_8$	7.03	22.18	3.52	1.388	1.384
MASPO	7.04	3.139	3.571		
MAPO	7.14	3.245	3.515		

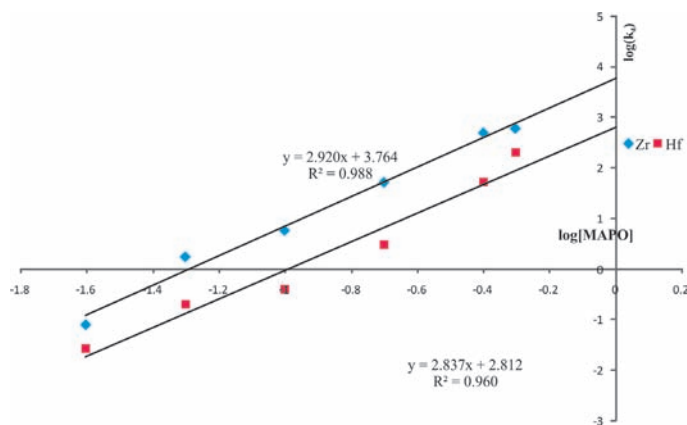


Fig. 4: Plot of $\log[K_d]$ versus $\log[\text{Extractant}]$.

Table 4: Experimental K_d for Zr^{4+} and Hf^{4+} with MAPO and MSAPO ligands.

Extractant	Feed (gpl)		K_d (Zr^{4+})	K_d (Hf^{4+})	SF(Zr/Hf)	Selectivity factor [$SF_{(Zr/Hf)MAPO} / SF_{(Zr/Hf)MSAPO}$]
	Zr^{4+}	Hf^{4+}				
0.1 M MAPO	1.2	0.6	12	0.60	20	1.65
0.1 M MSAPO	1.4	1.5	3.50	0.29	12.06	

The experimentally observed value was found to be in good agreement with the theoretically predicted extraction energy. The experimental K_d for Zr^{4+} ion is found to be always higher than Hf^{4+} ion for all the extractants as predicted by the theoretical calculation. The theoretical separation (SF) factor can be expressed in terms of the difference ($\Delta\Delta E$) between the extraction energy of Zr^{4+} ion (ΔE_{Zr}) and Hf^{4+} ion (ΔE_{Hf}), whereas experimentally, separation factor is determined from the ratio of K_d of Zr^{4+} ion and Hf^{4+} ion. The theoretically calculated separation factor which dictates the selectivity of the metal ion towards a particular extractant is found to be in good agreement with the experimentally observed selectivity of Zr^{4+} ion over Hf^{4+} ion. MAPO shows higher selectivity over MSAPO for Zr^{4+} ion over Hf^{4+} ion.

Conclusions

The preferential extraction of Zr^{4+} ion over Hf^{4+} ion towards organophosphorus extractants has been established using molecular modeling and solvent experiment studies. Density Functional theory successfully captures the higher complexation stability of MAPO over MSAPO for both Zr^{4+} and Hf^{4+} ions as observed in the solvent extraction experiment. The calculated extraction energy follows the same order of distribution constant which shows that MAPO is the best extractant in terms of high distribution constant. Further, the theoretically calculated separation factor which dictates the selectivity of the metal ion towards a particular extractant is found to be in excellent agreement with the experimentally observed selectivity of Zr^{4+} ion over Hf^{4+} ion. MAPO shows higher selectivity over MSAPO for Zr^{4+} ion over Hf^{4+} ion and hence promising for mutual separation of Zr^{4+} and Hf^{4+} ions. The calculated theoretical value of selectivity factor was found to be 1.37 which is very close to the experimentally determined value of 1.65.

Acknowledgement

We are thankful to Dr. S.B. Roy, Associate Director, ChEG for continuous support and encouragement. Anupam Supercomputer of BARC was used for all the computations.

References

- Gupta, C.K., Chemical Metallurgy: Principles and practice, Willy VCH, 2003.
- Levitt, A.E.; Freund, H., J. Am. Chem. Soc. 1956, 78, 1545.
- Gupta, B.; Poonma, M.; Niti, M., Solv. Ext. Ion Exch. 2005, 23, 345.
- Biswas, R.K.; Hayat, M.A., Hydrometallurgy 2002, 63, 149.
- Reddy, B.R.; Kumar, J.R.; Reddy, A.V.; Priya, N.D., Hydrometallurgy, 2004, 72, 303.
- Sato, T; Watanabe, H., J. Inorg. Nucl. Chem. 1974, 36, 2585.
- Suriyachat, D.; Distin, P.A.; Logsdail, D.H.; Slater, M.J. Elsevier Applied Science: London, 1993, 1, 265.
- Da Silva, A.B.V.; Distin, P.A. Jr., CIM Bulletin, 1998, 91, 221.
- Da Silva, A.B.V.; El-Ammouri, E.; Distin, P.A., Can. Metallurg. Q. 2000, 39, 37.
- Lee, H.Y.; Kim, S.G.; Oh, J.K., Hydrometallurgy, 2004, 73, 91.
- Blazheva, V.; Federov, Y.S.; Zilberman, B.Y.; Mashirov, L.G., Radiochemistry, 2008, 256-260.
- Nayl, A.A.; El-Naid, Y.A.; Daoud, J.A., Sep. Sci. Tech. 2009, 44, 2956.
- Ali, Sk. M., Eur. J. Inorg. Chem. 2014, 9, 1533
- Cramer, C.J., Essentials Of Computational Chemistry, John Wiley and Sons, 2004.
- Ahlich, R., Bar, M., Haser, M., Horn, H., Kolmel, C., Chem. Phys. Letters, 1989, 162, 165.
- Andrae, D.; Haeussermann, U.; Dolg, M.; Stoll, H.; Preuss, H. Theo. Chim. Acta. 1990, 77, 123.
- Becke, A.D., Phys. Rev. A 1988, 38, 3098.
- Perdew, J.P., Phys. Rev. B 1996, 33, 8822.
- Lee, C., Yang, W., Parr, R. G., Phys. Rev. B 1988, 37, 785.
- Klamt, A., J. Phys. Chem. 1995, 99, 2224.
- Schaftenaar, G.; Noordik, J.M., J. Comp. Aid. Mat. Des. 2000, 14, 123.
- Pearson, R.G., Inorg. Chem. 1988, 27, 734.
- Parr, R.G., Yang W. Density functional theory of atom and molecules, Oxford University Press, New York, 1989.
- Parr, R.G.; Pearson, R.G., J. Am. Chem. Soc. 1983, 105, 7512.

Optimization of Indigenously Developed Column for the Separation and Analysis of All the Six Hydrogen Isotopic Combinations in Elemental form using Gas Chromatograph

M. Ravichandran, P.R. Ramya, S. Sankar Ganesh, K.Ramesh Naidu and M.M. Rajput

Additional Upgrading Facility (AUGF)
Bhabha Atomic Research Centre, Kalpakkam

Abstract:

Monitoring the concentrations of the hydrogen isotopes at various stages is highly important to stabilize and maintain the process parameters in a detritiation plant. Gas chromatograph equipped with the in-house prepared column was used for the analysis of gas mixtures containing Hydrogen isotopes, which employs two main factors; separation of these gases based on their affinity for the stationary phase and the substantial difference in their thermal conductivities. The column was prepared using treated γ -Alumina as a stationary phase and packed in 1/8" SS tube of length 2.4 meter. Further the column was optimized and its performance study was carried out using Helium as carrier gas.

In this paper we have discussed the procedure of optimization and the performance of indigenously prepared column for the separation of H₂, HD, HT, D₂, DT and T₂ using gas chromatograph.

Keywords: H₂; Hydrogen; D₂; Deuterium; T₂; Tritium; HD; HT; DT; Isotopic analysis; Alumina column; Gas chromatograph(GC).

Introduction

For the stabilized operation of detritiation plant it is highly essential to monitor the hydrogen isotopes at various stages in the process. This can be performed by gas chromatographic analysis with more accuracy and effectively.

The heart of the gas chromatograph is the column, which performs the separations of the gaseous mixture and the individual component gases are detected at the detector end. The hydrogen isotopes analysis application lead us to the preparation of the column, which was packed with the in-house prepared stationary phase (γ -Al₂O₃ treated with iron oxide) and wounded into spiral coil of diameter 2.5 inch. Further we have worked in optimization of the stationary phase for obtaining satisfactory results.

Experimental

The essential parameter settings of the gas chromatographic systems like detector, injector and the column are listed in the Table -1.

The material used for making the column was of 1/8 inch size, 2.4 meter long SS 304 L tube. Prior to packing & winding into a coil form, the tube was cleaned with water and then dried, followed by flushing with acetone. The tube

Table 1: GC parameters

Carrier gas	Helium (Grade 5.0)
Carrier gas Flow rate	30-40 mLPM
Column	In-house prepared column (Al ₂ O ₃ treated with iron oxide)
Column Temperature	77K (dipped in LN ₂)
Injector temperature	50° C
Detector	Thermal Conductivity Detector
Detector temperature	50° C
Detector Voltage	8mV

was purged with helium gas and tested for leakage using MSLD. This cleaning and leak testing was performed to ensure integrity of the tube during analysis under varying temperature conditions.

The stationary phase was prepared by treating γ -Alumina with iron oxide; the resulting slurry was decanted, washed with demineralized water continuously, pH adjusted to neutral and sieved using 80-100 mesh size to collect uniform particles. The stationary phase thus prepared was carefully packed in the pre-cleaned & dried SS tube, which was then wounded into a spiral coil. This spirally wounded SS coil containing the in-house prepared stationary phase was used as the Gas Chromatography column for the analysis of hydrogen and its isotopes.

Optimization:

The Column immediately after packing was connected to the gas chromatograph for establishing the flow through it, after confirming the flow of carrier gas the whole column was immersed into Dewar flask containing liquid nitrogen (77 K), this was done to check the carrier gas flow through the stationary phase under 77 K temperature. Gas Chromatograph was allowed to stabilize by setting the parameters as in table-1. When the base line was stabilized exactly one ml of the sample mixture containing Hydrogen deuteride (HD) & Deuterium (D_2) was injected using the automatic gas sampling valve into the column. A single peak was observed at a retention time of about 4 minutes. This can be observed in the Fig.1, which shows no separation occurred at this stage.

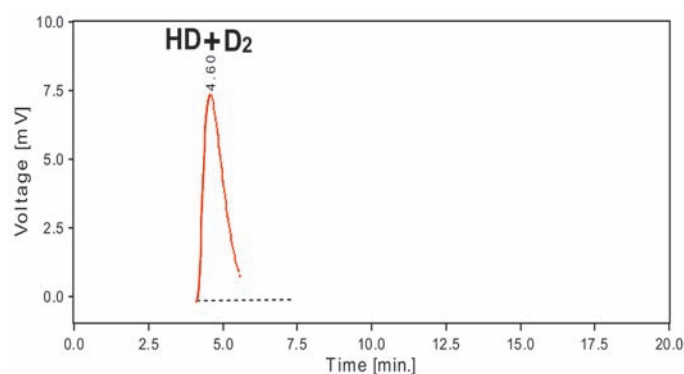


Fig.1 : Unresolved Chromatogram of (HD + D_2) mixture

Hence the column was removed from the liquid nitrogen dewar flask and it was heated to 150° C in the gas chromatograph oven with helium gas flow for about 24 hrs. After heating treatment, the column was again set for isotopic analysis with the sample mixture containing Hydrogen deuteride (HD) & Deuterium (D_2), a partial separation of the two isotopes was observed which can be viewed in Fig.2

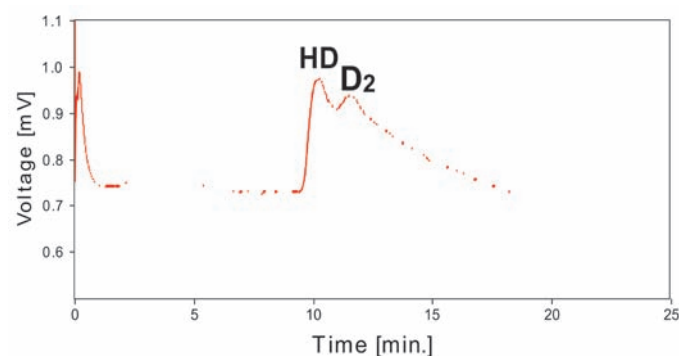


Fig. 2 : Partially separated chromatogram of (HD + D_2) mixture

Further to achieve better resolution of peaks, the column was disconnected from the gas chromatograph and heated in an oven at a temperature of about 180° C without carrier gas flow for 12 hrs. After conditioning in oven the column was connected to gas chromatograph for regeneration of the column with carrier gas flow at 150° C for about 8 hrs.

After regeneration, analysis was performed with the same sample mixture. We had observed two broadened peaks of Hydrogen deuteride (HD) & Deuterium (D_2) at retention times 16.41 minutes and 45.05 minutes respectively. The separation between HD and D_2 was about 28.64 minutes apart, which can be observed in Fig.3

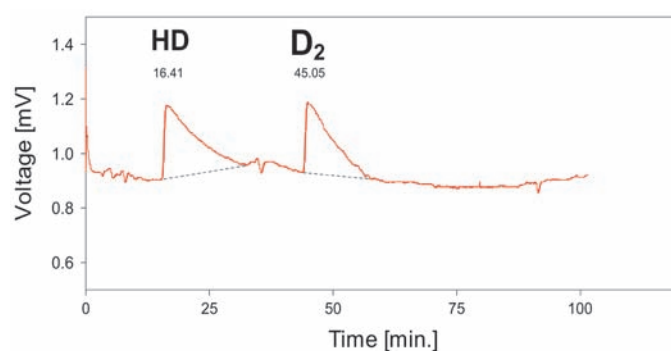


Fig.3 : Resolved Chromatogram of (HD + D_2) Mixture

At this stage of optimization, it is proved that the stationary phase prepared in-house, can separate hydrogen isotopes. But to have a smooth and well resolved peak separation further optimization was required.

We understood that the adsorption sites in the stationary phase are highly enhanced, hence HD and D_2 peaks are too apart. In order to optimize the adsorption sites in the stationary phase for better resolution, deactivation was done by passing CO_2 gas through the column.

Again the column was subjected to the direct heating procedure in the oven without carrier gas flow at 180° C for about 2 hrs. When direct heating is completed, the column was finally conditioned in the gas chromatograph oven with carrier gas flow at 150° C for about 2 hrs.

After the above procedure of pretreatment, the column was immersed into liquid nitrogen dewar flask and the column was subjected to isotopic analysis with the sample mixture containing HD & D_2 by maintaining the optimized analysis parameters given in Table-2.

Table 2: Optimized GC Parameters

Carrier gas	Helium (Grade 5.0)
Carrier gas Flow rate	30 mLPM
Column	In-house prepared column (Al ₂ O ₃ treated with iron oxide)
Column Temperature	77K (dipped in LN ₂)
Injector temperature	50° C
Detector	Thermal Conductivity Detector
Detector temperature	120° C
Detector Voltage	8mV

It was observed that the peaks of HD and D₂ were well separated as shown in the Fig. 4.

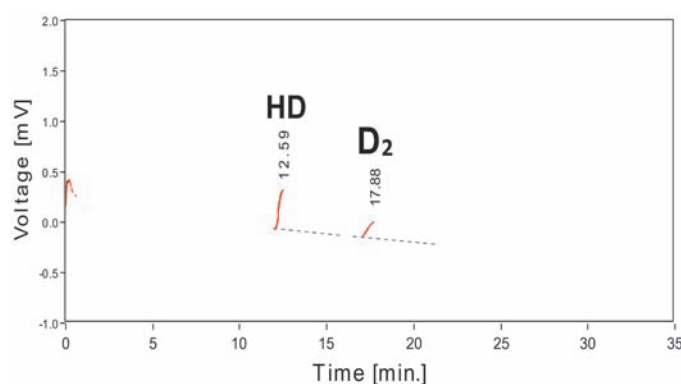


Fig. 4 : Well separated chromatogram of (HD + D₂) mixture

To check the performance of the column, samples from various systems and random mixtures were analysed and the respective chromatograms are observed as shown in the Fig.5 and Fig.6

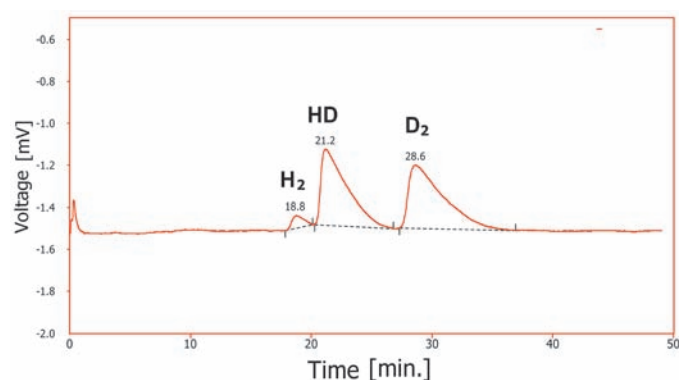


Fig.5 : Chromatogram of sample from collection tank showing good separation of H₂, HD and D₂ peaks

Results and conclusion

A satisfactory optimization of the in-house prepared Alumina column was achieved with respect to the temperature, carrier gas flow and stationary phase performance and thus

resulting in the separation and analysis of all six elemental forms of hydrogen isotopic combinations which is shown in the Fig.6

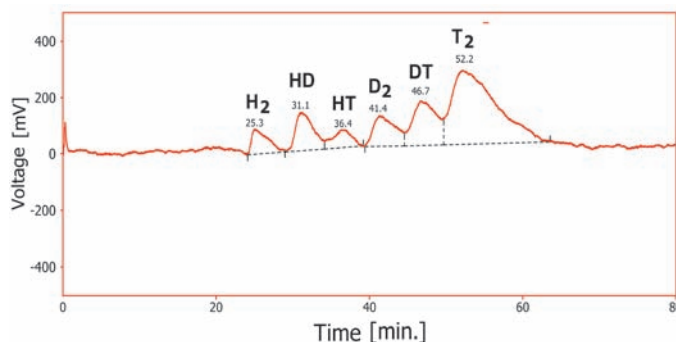


Fig.6 : Chromatogram of a Sample mixture showing the separation of H₂, HD, HT, D₂, DT and T₂ peaks

Table-3: Column performance data for the chromatogram in Fig. 6

Component	tR (min)	W _{1/2} (min)	W (min)	R	N	H (mm)
H ₂	25.25	2.67	4.87	-----	496	4.838
HD	31.14	2.58	5.17	1.32	807	2.974
HT	36.43	2.83	5.05	1.15	919	2.611
D ₂	41.38	3.76	5.15	0.88	670	3.582
DT	46.71	4.21	5.12	0.78	681	3.524
T ₂	52.24	6.35	13.93	0.61	375	6.400

The analysis with helium as carrier gas was good enough in the separation of the hydrogen isotopes, but the peak height of the constituents were observed to be very small. Hence sensitivity is required to be improved without disturbing the separation process.

A carrier gas like Neon, which has greater thermal conductivity difference with respect to hydrogen isotopes could be suitable for achieving high sensitivity, Hence further research studies are needed to be carried out using Neon as carrier gas for the isotopic purity analysis of hydrogen isotopes.

Further studies on the in-house prepared Alumina column are needed to be carried out in the separation and analysis of Helium-3(decay product of Tritium) from the hydrogen isotopes mixture.

Comparison of responses of hydrogen isotope with different detectors (TCD & ICD), experiments with Neon as carrier gases and Separation & analysis of He-3 would be studied

as continuation of this work with the in-house prepared and optimized Alumina column.

Acknowledgment

We gratefully acknowledge the technical support received from Shri P.V.S. Aditya, Shri S. Ayyanar, Shri K.C. Sajith and thankful to the operation crews of AUGF for supporting during the course of work.

The contribution of Shri M. Thirumalaiselvan Shri P. Venkatachalam, Shri K. Parthiban, Shri T. Ramesh of maintenance services of AUGF during fabrication of the column and providing gas loop tubing & connectivity fitting arrangements throughout the experiment is deeply acknowledged.

Reference

1. Yoshinori Kawamura*, Yasunori Iwai, Toshihiko Yamanishi, Satoshi Konishi, Masataka Nishi (2000), Analysis of hydrogen isotopes with a micro gas chromatograph.
2. Yoshinori Kawamura *, Satoshi Konishi, Masataka Nishi (2001), Development of a micro gas chromatograph for the analysis of hydrogen isotope gas mixtures in the fusion fuel cycle
3. Edward H. Carter, JR., and Hilton A. Smith (January 11, 1963), The Separation of Hydrogen, Hydrogen Deuteride, Tritium Hydride, Deuterium, Tritium Deuteride And Tritium Mixtures By Gas Chromatograph
4. Kuniaki Watanabe*, Masao Matsuyama, Tohru Kobayashi, Wei Min Shu (1998) Hydrogen isotope separation by gas chromatography using Pd – Pt alloy
5. Yeshwant Naik, G.A. Rama Roa, V. Venugopal, Bhabha Atomic Research Centre, Mumbai (2000). Separation of hydrogen isotopes by gas chromatograph using vanadium oxide coated molecular sieve (4A) packed column.
6. M. Venugopal And K.O. Kutschke (1963), Gas Chromatographic Separation Of Hydrogen Isotopes On Activated Alumina.
7. Y.P. Naik, N.K. Gupta, K.T. Pillai, G.A. RamaRao, V. Venugopal, Product Development Division, Bhabha Atomic Research Centre, Mumbai, India. (2011) Gas Chromatographic Separation Of Hydrogen Isotopes On Columns Packed With Alumina, Modified Alumina And Sol- Gel Alumina.
8. Dave, Sharad M.; Sadhukhan, Himangshu K. (Bhabha Atomic Research Centre, Mumbai (India); Novaro, Octavio A. (Instituto de Fisica, Universidad Nacional Autonoma de Mexico, Mexico) 1997, Heavy water: properties, production and analysis (Quest Publication), Mumbai.
9. IAN A. FOWLIS, Gas Chromatography- Analytical Chemistry By Open Learning- 2nd Edition (Published By John Wiley & Sons).
10. HAROLD M. McNAIR, JAMES M. MILLER, Basic Gas Chromatography (Published By John Wiley & Sons).

Radiation Technology for Sewage Sludge Hygienisation

Lalit Varshney

Radiation Technology Development Division

Abstract:

Large amount of sewage sludge is produced in India every day. The sludge is infectious and can spread diseases. It also has essential micro and macro nutrients, especially carbon, useful for soil and crop production. Radiation Technology can be used to hygienise the sludge reliably and affordably and protect health and environment. Addition of useful microorganisms to the hygienised sludge can convert it to a value added manure. Ahmedabad Municipal Corporation (AMC) takes the lead to set up first plant in India to treat 100 tons/day sludge and produce manure using a fully automatic process.

Introduction

A significant fraction of India's population of more than 1.2 billion lives in urban areas, where sewage is collectively treated in Sewage Treatment Plants (STP). Sewage is the waste water generated mainly from domestic premises. It typically contains 99.95% water and about 0.05% solid comprising organic and inorganic matter. During its journey to STP, sewage gets contaminated by chemicals, pharmaceuticals, insecticides, pesticides, heavy metals, etc from different sources. Although, large volume of the sewage dilutes their concentration, it needs to be controlled by regulatory authorities. Presently, about 38 billion litres of sewage is generated every day in India. Less than half of it is treated scientifically at STPs before it is discharged to larger water bodies (1). At STP, water and solid components are separated through primary and secondary treatments (aerobic digestion, activated sludge process). The thickened sludge from the digesters is sun dried or filter pressed to form dry sludge. Aerobic digestion is achieved by growth of selected microorganisms in presence of oxygen. During the growth, the organic matter is decomposed to simpler forms and the sludge is stabilised. Disposal of sewage sludge, especially in large cities is a serious problem for authorities as it contains a high load of potentially infectious microorganisms, a serious threat to public health. Currently, the sludge is land filled or given to farmers. This practice results in spread of diseases and contaminates ground water. There are strict norms for sludge disposal and its land applications in developed countries. Government of India, ministry of urban development has recently published recommendations for sludge disposal which are similar to those of United States Environmental Protection Agency (USEPA)[1,2].

Interest in sludge utilisation for agriculture has increased among the farming community. Dry sludge, when added to soil, provides macro and micro nutrients such as C, N,

P, K and Zn, Fe, Cu etc., improve soil physical properties and above all increase the soil organic matter resulting in increased crop productivity as well as restoration of soil fertility. For STP operators, it is a value added by-product from waste whose disposal, otherwise, is a matter of environmental concern. Therefore, recycling the sludge for agriculture applications can emerge as an important activity provided it is carried out in a manner that protects human and animal health as well as environment at large.

Radiation technology is a promising technology being explored in many countries for hygienising sewage sludge. In India, a demonstration facility to hygienize liquid sludge (96% water and 4% soil) is operating in Vadodara, Gujarat for more than 20 years and the local agricultural institutes have established the use of hygienised sludge for crop production [3]. However, the sludge produced by the process is uneconomical and not conducive to large scale operation. Directly hygienising dry sludge in the present process is more economical, reliable, scalable and gives better quality sludge.

Radiation Technology and disposal norms for sewage sludge:

Ionizing radiation emitted by radiation source such as Cobalt-60 interacts with the critical molecules like DNA, proteins and water present in the cell and result in the inactivation of microorganisms. Some of the pathogens present and their number in the sludge are listed in Table 1. As a result of Irradiation, besides pathogens, other unwanted constituents like weeds, chemicals, etc. are also degraded, making the sludge safer for use (Table 2). Based on microbiological inactivation, Radiation Technology is already established world over for sterilizing medical products, food safety and food preservation. Sludge hygienisation can be carried out in the similar manner.

As per the established norms, the STP sludge should be hygienised before it can be applied on land or ginen

Table 1: Typical pathogens present in sludge and their numbers.

Microorganism	Concentration(number)/g
Coliform	10 ⁵ -10 ⁷
Fecal coliform	10 ⁴ -10 ⁶
Fecal streptococci	10 ⁴ -10 ⁵
-Salmonella	1-100

Table 2: Effects of gamma radiation on Polyaromatic Hydrocarbons (PAH) in sewage sludge * IAEAtecdoc 1317, page71, 2002 [2]

Dose in kGy	Moist Sludge mg/kg [% degradation]	Dry sludge mg/kg [% degradation]
Control	29	5.5
2.0	13.7 [53]	4.4 [26]
4.0	6.8 [77]	2.4 [56]
6.0	6.1 [79]	3.1 [43]
8.0	10.1 [65]	2.8 [47]
10.0	7.2 [75]	2.0 [63]

in container/bags to the users. Lime stabilization, heat pasteurization, composting, mesophilic and thermophilic digestion are some of the methods currently practiced. Treatment by these methods converts the sludge to "Biosolid A", which does not invite several restrictions required otherwise for use of untreated sludge[2]. The sludge for land application should not exceed the specified limits for:

1. The presence of pollutants (Arsenic, cadmium, chromium, copper, lead, mercury, nickel, selenium and zinc). Domestic sewage is not expected to have high concentration of these metals. Ministry of Urban Development (MoUD) and United

States Environmental Protection Agency (US EPA, 40CFR 503,) have described similar ceiling limits(Table3). Radiation processing does not alter the concentration of heavy metals.

2. The presence of pathogens (e.g. bacteria, viruses, parasites, helminth ova etc)

3. The sewage sludge attractiveness to vectors e.g. rodents, flies, mosquitoes, birds etc. which could transfer pathogens to other places and human. STP process and sun/heat drying reduce this factor.

US EPA and MoUD guidelines have described gamma and electron beam irradiation as effective methods to further reduce pathogens in STP sludge [1,2]. Sludge as such is very difficult to characterize in terms of microbiological and chemical loads which keep changing [4]. Irradiation ensures that sludge does not contain pathogens. Other solid wastes can also be hygienised using the process of dry sludge irradiation.

An average radiation dose of 8-10 kGy is required to hygienise dry sludge [5]. A standard configuration of a city STP along with irradiation facility is shown in Fig. 1.

The schematic of the dry sludge hygienisation process is shown in the Fig. 2. The dry sludge containing about 75% solid is brought to irradiation facility in dumpers and poured into the crushers. The crushed sludge is carried by conveyor belt to aluminium tote boxes and filled. The tote boxes are irradiated at 8 - 10 kGy. The hygienised powder sludge is inoculated with useful bacteria through automated spray unit containing the liquid bio-fertilizer. The inoculated sludge is filled in 50 kg bags at bagging station and sealed. Quality assurance is done by batch wise measuring microbiological population and heavy metal concentration in the sludge before and after irradiation. Re-growth possibility

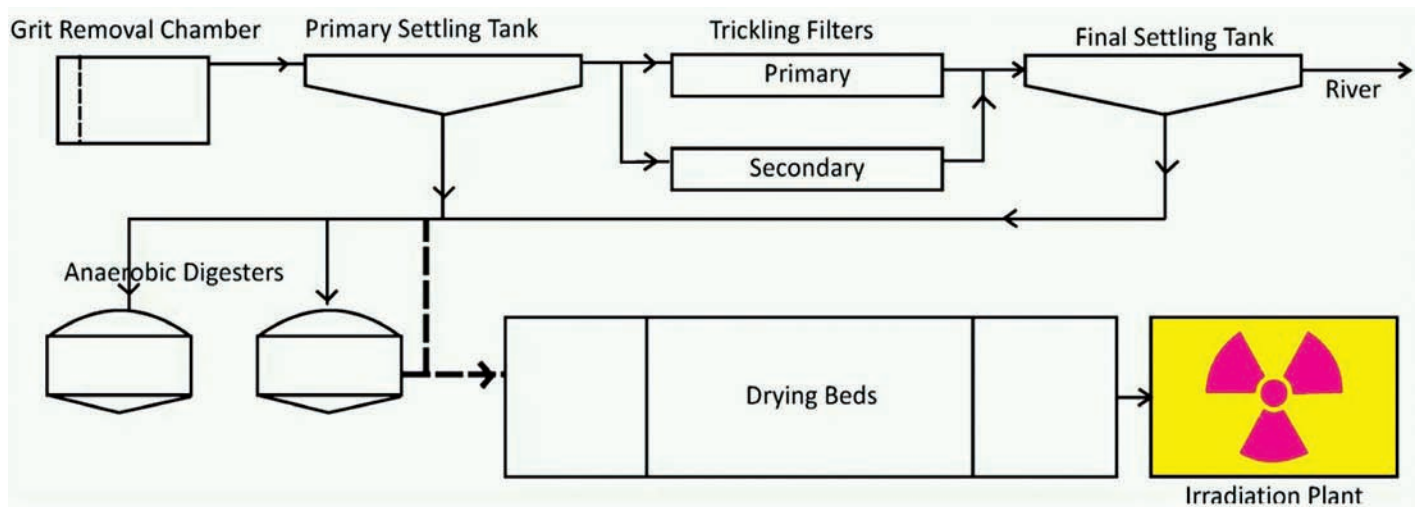


Fig. 1: A standard STP facility along with Irradiation facility

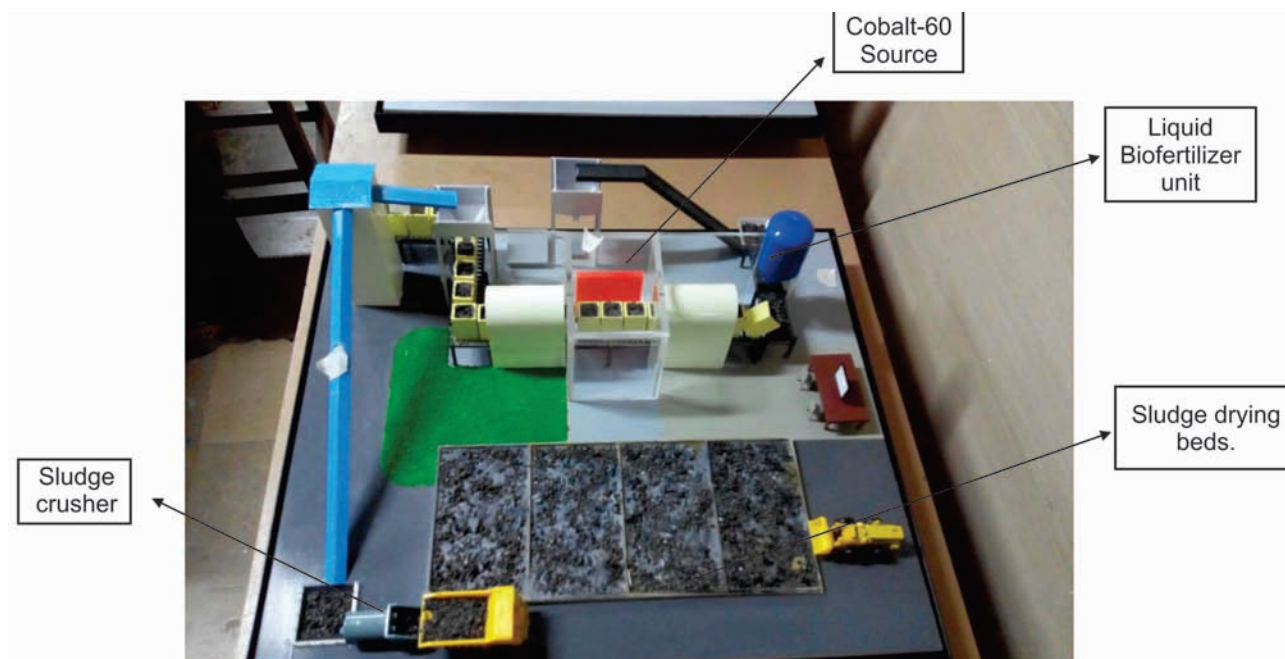


Fig.2 : Process flow sheet diagram for 100 tons/day facility

of pathogens in hygienised dry sludge in sealed bags is negligible [6]. A typical heavy metal ion concentration in dry sludge given in Table 3 shows that the concentration of the heavy metal ions are much below the ceiling limits. The hygienised sludge can be safely transported and stored in bags for longer time.

Table 4. shows killing of coliforms (including fecal coliforms) in irradiated 50 kg sludge bags. Inactivation of fecal coliforms which are generally present in large number indicates destruction of pathogens. Highly radiation resistant Bacillus

Pumilus spores (Table 4) could also be used to further establish efficacy of radiation process for hygienisation.

The reduction in microbial population in radiation treated sludge results in lower microbial competition for sludge nutrients. This enables more growth of inoculated useful microorganisms in the sludge converting it into bio-fertilizer. Use of such sludge improves availability of N,P,K in soil to plants. Table 5. shows results of inoculation of irradiated sludge with useful microorganisms and their population. The inoculation process is carried out after sludge hygienisation.

Table 3: Typical elemental analysis of AMC STP plant's dry sludge.

Element	Ceiling Concentration	AMC 180 MLD STP	AMC 240 MLD STP
Total organic Carbon(Weight %)	-	41.27	39.76
Copper (mg/kg)	4300 [75]*	277.5	20.5
Nickel(mg/kg)	420 [21]	39.4	14.9
Zinc (mg/kg)	7500 [140]	667	198.6
Lead(mg/kg)	840[15]	23.6	4.8
Cadmium(mg/kg)	85[1.9]	9.8	0.6
Chromium(mg/kg)	3000[150]	80.6	10.1
Mercury(mg/kg)	57[0.85]	BDL	BDL
Arsenic(mg/kg)	75[20]	BDL	BDL
Nitrogen (mg/kg)	-	116.2	178
Potash(K ₂ O) (mg/kg)	-	301.2	409
Phosphorous(P ₂ O ₅) (mg/kg)	-	34.7	22.4
pH	-	7.14	7.52

*= Figures in parenthesis indicate annual pollutant loading rate in kg/hectare on land[2], BDL: below detection limit, MLD : million liters per day

Table 4. Inactivation of coliforms and B.Pumilus spores on dry sludge irradiation

S.No.	Dosimeter position in the bag	Radiation dose(kGy)	Coliform/g	Bacillus Pumilus Spores
1.	Control	0.0	11.5 x 10 ⁵	1 x 10 ⁶
2.	Minimum (Centre)	6.85	Nil	0.96x 10 ²
	Maximum(Surface)	9.03	Nil	0.30 x 10 ²
3.	Minimum(Centre)	7.07	Nil	0.42 x 10 ²
	Maximum(Surface)	9.15	Nil	0.16 x 10 ²
4.	Minimum(Centre)	6.81	Nil	0.85 x 10 ²
	Maximum(Surface)	9.04	Nil	0.10 x 10 ²

Table 5: Number of useful bacteria in unhygienised and hygienised sludge after inoculation with equal quantities of inoculum

Useful bacteria	Inoculation in non irradiated sludge	Inoculation in Irradiated sludge
Phosphate solubilizing	3 x 10 ⁹	5 x 10 ¹¹
Rhizobium	2.5 x 10 ⁸	2.5 x 10 ¹¹
Azotobacter	4 x 10 ⁹	2.5 x 10 ¹²

Advantages of Radiation Technology:

The various Advantages of Radiation Hygienisation of Dry Sewage Sludge Process are listed below:

- Process is simple, economic, effective, reproducible and scalable.
- Easy to integrate with conventional sewage treatment facilities.
- Process is fully automatic to avoid manual handling of contaminated sludge.
- Based on the process of radiation sterilization which is well established world over and in India.
- Degrades chemical contaminants and makes sludge safer for use.

Benefits to the farmers/people:

Various benefits to farmers on using radiation hygienised sludge are:-

- Increased crop yield - direct benefit to the farmers.
- Improved soil conditions - soil conservation & restoration.
- Reduced health risks associated with sludge, reduces costs of health care system.
- Reduced demand of water due to higher water holding capacity of the sludge.

- The nutrient rich sludge, which otherwise is discarded, can be gainfully recycled for economic gain.
- Improved overall quality of life.

MoU with AMC, Ahmedabad

Bhabha Atomic Research Centre entered into an MoU on 21st April, 2015 with Ahmedabad Municipal Corporation (AMC) to provide all technical and scientific support for setting up a Cobalt -60 Gamma Irradiation Plant at Ahmedabad. On 30 January, 2016, Chief Minister of Gujarat, Smt. Anandiben Patel laid the foundation stone for 1.5 Million Curies Co-60 irradiation facility (Fig.3). The fully automatic facility can hygienise 100 tons of dry sludge every day. The hygienised sludge inoculated with useful bacteria will provide a value added bio-fertilizer. The product will be marketed by Gujarat Agro Industries Corporation(GAIC) as per separate MoU between AMC and GAIC.

Future prospects of Radiation Technology for sludge hygienisation:

Radiation Technology applications are increasingly being employed for sustainable development. Directly hygienising sewage may not be an economical solution as volumes concerned for treatment are huge. Dry sludge component is only 0.05% but still it leads to generation of very large quantities of dry sludge every day posing a serious problem of its disposal. Considering its nutrient value, it is better to gainfully recycle it for land applications. Value added products/formulations can be made using hygienised sludge along with useful bacteria, sea weeds and other wastes(organic and inorganic). Although setting up a sludge hygienisation facility may not be a business model (radiation sterilization facilities can be more profitable) but municipalities can run it with marginal profit and could indirectly benefit masses by protecting the environment and health. The money value of such benefits can not be determined. India has an ambitious nuclear power program



Fig. 3: Chief Minister of Gujarat during Foundation Stone laying function on 30th January 2016 at Ahmedabad. Addressing the gathering (left) and with BARC officials(right).

and as a result availability of Cobalt-60 is assured for many years through Board of Radiation and Isotope Technology (BRIT). A gamma irradiation facility of 100 tons/day capacity cost about 25-30 crore rupees and require an area of 4500 square meter. The sludge treatment cost per kg is less than one rupee. A 100 tons/day facility caters to a city of about 2-3 million population. This makes putting up facilities where sludge generation is small unviable as civil and machinery are fixed cost for such a facility, big or small. However, a single facility of 100 tons/day could cater to cluster of towns each generating 2-5 tons of sludge per day. The first plant in Ahmedabad is expected to be commissioned by 2017 in and another 15-20 plants by 2030 are achievable. Technology and Cobalt source both are indigenously available. Ongoing indigenous Electron beam accelerator program of DAE would be able to supplement the increased demands for such plants in future. With the Government of India's new focus on development technologies for Swachh and Swasth Bharat, Radiation Technology is a promising technology which can contribute gainfully to achieve this objective and protect health and environment.

Conclusions

Radiation technology has sound scientific basis and is a practical technology to economically hygienise sewage sludge for agriculture application. The technology and radiation source both are available in our country. Irradiation facility can be utilised to treat whole city sludge at one place in a fully automatic process. The hygienised sludge can benefit farmers and protect environment and human health. The technology has high potential in contributing towards meeting the objectives of Clean India Mission (the Swachh Bharat mission).

Acknowledgements

Author wishes to thank all those who contributed directly or indirectly to the growth of this technology for societal benefits.

References

1. Manual on sewerage and sewage treatment system, Ministry of Urban Development, PART A, Page no. 76-90, Nov. 2013, New Delhi(<http://mou.gov.in>)
2. United States Environmental Protection Agency(US,EPA), 40 CFR Part 503
3. Gamma Irradiation of Municipal Sewage Sludge for safe Disposal and Agricultural Use. Satyendra Gautam, M.R. Shah, Sunil Sabharwal and Arun Sharma,, Water Environment Research, Vol. 77, No. 5, Srep./Oct. 2005, 472-478,
4. Irradiated sewage sludge for application to cropland., IAEA-Techdoc-1317, Oct.2002
5. Sewage Sludge Hygienisation using Radiation Technology, Lalit Varshney, S.P. Kale and A.K. Kohli, Internal Report,2014, BARC, Mumbai40085.
6. Potential regrowth and recolonization of salmonellae and indicators in biosolid and biosolid amended soil. Kathleen J. Zaleski, Karen L. Josephson, Charles P. Gerba, and Ian L. Pepper, Applied and Environmental Biology, July 2005,71(7) 3701-3708.

For more information please contact: Head, Radiation TechnologyDevelopmentDivision,B.A.R.C.,Mumbai-400085, India. email:lalityv@barc.gov.in, Phone:91-22-2559374

Technology Transfer

During the period between February 2015 and April 2015, BARC has transferred Nine technologies to various industries. Technology Transfer & Collaboration Division (TT&CD) co-ordinated these technology transfers. The details are given below:

A. "DIP N DRINK MEMBRANE POUCH" technology was transferred to M/s. S. K. Mittal & Co. Pvt. Ltd., New Delhi on February 11th, 2015.

"Dip N Drink Membrane pouch" technology has been developed by Desalination Division, BARC. The Membrane Pouch is based on Osmosis process to get sterile drinkable solution from biologically contaminated water especially during disaster conditions like flood, cyclones, tsunami, earthquakes and useful for concentration of high value low volume product in food, pharmaceutical, chemical industries. It can also be used in Oral Rehydration Therapy in remote areas.

B. "ANUSPECT Gamma Spectrum Analysis software" Technology was transferred to M/s. Nucleonix Systems Pvt. Ltd., Hyderabad (A.P) on

The technology was developed by Electronics Division. ANUSPECT-Multi-core framework is for Gamma Spectroscopy. It is an integrated gamma spectroscopy data acquisition and spectral analysis software program. ANUSPECT software provides visually effective Graphical User Interface (GUI) for effortless Gamma Spectrum Analysis. It provides offline as well online spectrum analysis. It supports online spectrum analysis for USB MCA cards (based on Cypress EZ-USB-FX2), however, it can be made adaptable to other MCA cards. ANUSPECT has application fields ranging from laboratory gamma spectroscopy, waste measurement, fuel reprocessing, whole body counting and nuclear safeguards.



Photograph after signing the agreement with M/s S. K. Mittal & Co. Pvt. Ltd., New Delhi seen from left to right, Shri G. R. Ursal, TT&CD, Dr. A. K. Ghosh, MDS, DD Dr. R. C. Bindal, Head, MDS, ChEG, Dr. (Smt.) S. B. Roy, Associate Director, Chemical Engineering Group, Shri G. Ganesh, Head, TT&CD, Shri Rajat Mittal, Director, M/s S. K. Mittal & Co. Pvt. Ltd., Shri D. Goswami, Head, DD and Shri S. K. Mittal, Director, M/s S. K. Mittal & Co. Pvt. Ltd



Photograph after signing the agreement with M/s. Nucleonix Systems Pvt. Ltd., Hyderabad seen from left to right, Sh. Mahesh P, ED, Smt Padmini S, ED, Sh D. Das, Head, ED, Sh J. Narendra Reddy, Managing Director, M/s Nucleonix Systems Pvt. Ltd., Hyderabad, Sh. J. Nishanth Reddy, Director IT, M/s Nucleonix, Sh G. Ganesh, Head, TT&CD & Smt Preeti K Pal, TT&CD

C. "A rapid, continuous and renewable method for production of the anti-cancer drug Camptothecin" to M/s Pratyaksha Agrotech Pvt. Ltd., New Delhi, on March 11th, 2015.

This technology has been developed by Nuclear Agriculture & Biotechnology Division (NA&BTD). It is a Plant tissue culture

method for the continuous and enhanced production of the anticancer quinoline alkaloid camptothecin using multiple shoot cultures of *Ophiorrhiza rugosa* var *decumbens*. The yield of camptothecin in the cultures is found to be 0.056 % dry weight during a period of 35 days and the parent plant contained 0.002 % dry weight.



Photograph after signing the agreement with M/s S. K. Mittal & Co. Pvt. Ltd., New Delhi seen from left to right, Dr S P Kale, Head, NA&BTD, Shri G Ganesh, Head TT&CD, Shri Supratim Roy Choudhury, Director, M/s Pratyaksha Agrotech Pvt. Ltd., New Delhi, Dr Roja Gopalkrishnan, NABTD and Smt S Mule, TT&CD

D. Technologies of “Quadrupole Mass Spectrometer”, “Passive Catalytic Recombiner Device” and “Cobalt-60 Teletherapy Machine” were transferred to M/s ECIL, Hyderabad on April 15th, 2015

• **Quadrupole Mass Spectrometer**

The Quadrupole Mass Spectrometer is a very versatile analytical instrument, developed by Technical Physics Division, BARC that is capable of compositional analysis of gases and volatile liquids. It consists of an Electron Impact ion source, quadrupole mass analyzer and a detector. It can analyse a mass range of 1-300 amu with a resolution of 1 amu, which is adjustable.

• **Passive Catalytic Recombiner Device**

As part of the hydrogen mitigation technology development programme being pursued at BARC, a catalytic recombinder device has been developed using different types of noble-metal based catalysts. These devices have been experimentally evaluated for their performance in the Hydrogen Recombiner Test Facility (HRTF), Tarapur in collaboration with NPCIL. On the basis of the results obtained from these experiments, the catalyst developed by Chemistry Division of BARC has been found most suitable. This catalyst will be housed in a recombinder box developed at Reactor Safety Division, BARC to form a Passive Catalytic Recombiner Device (PCRD).



Photograph after signing technology transfer agreement of Quadrupole Mass Spectrometer (QMS). Shri P. Viswanath, Executive Director ECIL, signed the agreement on behalf of ECIL. Dr. S. L. Chaplot, Director, Physics Group, Dr. S. K. Gupta, Head, TPD and his Team were present on this occasion.



Photograph after signing technology transfer agreement of Passive Catalytic Recombiner Device. Shri P. Viswanath, Executive Director ECIL, signed the agreement on behalf of ECIL. Dr. B. N. Jagtap, Director, Chemistry Group, Dr. R. K. Singh, Associate Director & Head RSD, RD&DG, Shri S. G. Markandeya, OSD, Shri. G. Ganesh, Head, TT&CD, Dr. V. K. Jain, Head, Chemistry Division and his team were present on this occasion.

- **Cobalt-60 Teletherapy Machine**

Co-60 Teletherapy Machine is developed by Division of Remote Handling & Robotics, BARC for treatment of cancer. It uses Co-60 radiation source for treatment. The primary

design requirement for any radiation therapy system is to maximize the radiation dose to the tumor sites while minimizing the dose to all the surrounding normal tissues. This system has all the state of the art features to perform as per the international standards.



Photograph after signing technology transfer agreement of Cobalt-60 Teletherapy Machine. Shri P. Viswanath, Executive Director ECIL, signed the agreement on behalf of ECIL. Shri C. K. Pithawa, Director DM&AG, Shri Y. K. Taly, AD, DM&AG, Shri. G. Ganesh, Head, TT&CD, Dr. D. N. Badodkar, Head, DRHR and his team were present on this occasion.

E. "Soil Organic Carbon Detection Kit (SOCDK)" Technology was transferred to M/s Agriland Biotech Limited, Vadodara (Gujarat) on April 15th, 2014.

This technology was developed by Nuclear Agriculture and Biotechnology Division, BARC. This kit analyses organic carbon content of soil directly on the field. This kit has been devised to help farmers to understand the carbon status of his field which ultimately decides the yield of crop. It gives quick results and thereby enables farmer to take corrective measures for maintaining soil fertility especially before sowing and at the harvest of any crop. The detection method works on the basis of organic matter extraction from the soil. The extraction is enhanced by addition of chemicals provided in the kit. The colour developed after extraction shall be compared with chart provided for estimation of organic carbon content of the soil. Estimation of soil organic carbon content becomes easy to perform, giving immediate results and useful to farmers for their own use.

F. "70kJ, 25kV Electromagnetic Manufacturing Equipment (EME)" Technology was transferred to M/s Artech Welders Pvt. Ltd., Pune, (Maharashtra), on April 27th 2015.

This technology of was developed by Accelerator & Pulse Power Division, BARC. Electromagnetic manufacturing process is the state of art technology for shaping and joining of metals based on electromagnetic forming and electromagnetic welding. In these techniques, forming and welding are achieved without physical contact between tool and job piece. Hence it has obvious merits over conventional processes such as brazing, welding, expansion, contraction, contour formation etc., when used for some special applications. This sophisticated technique has many advantages such as precision, reproducibility, high production rate, no tool marks, minimization of manual error, automation ease, etc. The preparatory procedures such as preheating, lubrication, etc. are not needed.



Photograph after signing the agreement with M/s Artech Welders Pvt. Ltd., Pune, (Maharashtra), seen from left to right, Shri P.C. Saroj, APPD, Dr. (Smt) Archana Sharma, Head, PPSS, APPD, Shri R.K. Rajawat, Head, APPD, Dr. K. Dasgupta, AD, BTDG, Shri Subhash Patwardhan, Director, M/s Artech Welders Pvt. Ltd., Shri G. Ganesh, Head, TT&CD, Shri S.N. Dutta, TT&CD, Shri V. K. Upadhyay, TT&CD.

Electromagnetic Welding is suitable for 1mm thick flat sheets of various metals such as Al-Al, Al-SS, Al-Cu, and Al-Al (alloy). This technique has great potential in automobile, electric, defense, aeronautical and other industries.

G. Nisargruna Biogas Technology based on biodegradable waste has been developed by NA&BTD. The plant processes biodegradable waste into biogas and weed free manure. It was transferred to the following six parties :-

- M/s Vasundhara Services, Pune on 11.02.2015
 - M/s Green Power Solutions, Navi Mumbai on 19.02.2015
 - M/s CBS Technologies Pvt. Ltd., Delhi on 24.02.2015
 - M/s Aruna Green Ventures Pvt. Ltd., Bangalore on 12.03.2015
 - M/s Alfa-Therm Ltd., New Delhi on 08.04.2015
- M/s Eclean Spectron Environment Pvt. Ltd., Mumbai on 11.02.2015

20th National Seminar On Crystal Growth & Applications 2016 (NSCGA-2016): A Report

The '20th National Seminar on Crystal Growth and Applications' was organized by TPD, BARC during 19th to 21st January 2016 at the multipurpose hall, TSH. This was partially supported by the 'Board of Research in Nuclear Science (BRNS)' and the 'Materials Research Society of India - Mumbai Chapter (MRSI)'. This was the 20th in the series of such seminars dedicated to crystal growth and held at various universities working in this area of research. This was the first time that it was held at BARC. Dr. S. C. Gadkari, OS & Head CTS, TPD was the chairman NSCGA-2016 of the conference with Dr. Shashwati Sen acting as the Convener NSCGA-2016 and Dr. Mohit Tyagi the secretary NSCGA-2016.

Dr. Srikumar Banerjee, former Chairman, Atomic Energy Commission and Secretary to the Department of Atomic Energy (DAE), was the chief guest in the inaugural function. He also unveiled the proceedings of the seminar. Dr. S. M. Sharma, Director Physics Group gave the inaugural address and Dr S. K. Gupta gave the welcome address. The newsletter of Indian Association for Crystal growth was unveiled by Dr. G. P. Kothiyal, Chairman of MRSI-Mumbai Chapter. The industrial exhibition was inaugurated by Dr. R. K. Sharma, Director SSPL, New Delhi. The keynote address was given by Dr. V. Nagarkar, Vice-President, Radiation Monitoring Devices, USA.

Total 157 manuscripts were received from all over the country working on crystal growth and related fields. Manuscripts were invited under 8 different topics ranging from growth of single crystals, Nano crystals to devices based on single crystals for societal benefits. The application of crystals for device fabrication was specially emphasized in the seminar.

Around 150-175 participants from all over the country attended the seminar and presented their work. There were 15 invited talks given by eminent scientist coming from across the globe as well as throughout the country.

Beside this there were two evening talk given by Dr. S. K. gupta, Associate Director Physics Group BARC and Dr. B. N. Jagtap, Director Chemistry Group BARC. To synergize the interaction between the researchers and industry an industrial exhibition was also organized in which 10 companies participated. One local industry also gave industrial presentation pertaining to their products for crystal growth equipment.

The participants presented their work in the form of posters and 10 oral presentations. Participants also contributed in two award categories; 'Young Crystal Grower Award' and 'Best Crystal/Device Display Award'. There were four entries in each of these categories and two awards were given



Dr. S. Banerjee, Chief Guest, unveiling the seminar proceedings



Dr. S. K. Gupta Associate Director Physics Group BARC giving the evening Lecture



Award distribution by Dr. G. Amarendra, Director Materials Group IGCAR at the concluding session

in each of the above categories. Four best poster awards and two best oral award were also given to motivate the students to perform better.

The conference covered a wide range of topics in the field of single crystal growth, their applications and technologically

important devices based on the single crystals. Interesting devices showcasing the application of crystals were displayed at the conference. The participants were highly interested in the technological aspects and were keen to take up research which can have direct implications to society.



Modular Lab at BARC

Edited & Published by:
Scientific Information Resource Division
Bhabha Atomic Research Centre, Trombay, Mumbai 400 085, India
BARC Newsletter is also available at URL:<http://www.barc.gov.in>